Tumor edge architecture in glioblastoma is constructed by inter-cellular signals from vascular endothelial cells

Authors:

Soniya Bastola[1, 5†], Marat S. Pavlyukov[2†], Yasmin Ghochani[3], Sree Deepthi Muthukrishnan[3], Hee Jin Cho[4], Yeri Lee[4], Alireza Sohrabi[5], Stephanie K. Seidlits[5, 6], Daisuke Yamashita[7], Min Soo Kim[1, 3], Ksenia S. Anufrieva[8], Riki Kawaguchi[9], Yue Qin[9], Alma L Burlingame[10], Juan A. Oses-Prieto[10], Steven A. Goldman[11], Anita B. Hjelmeland[12], Do-Hyun Nam[13], Harley I. Kornblum[1, 15*], and Ichiro Nakano[5, 14, 15*]

Affiliations:

[1]Graduate Biomedical Sciences, University of Alabama at Birmingham, AL 35294, USA

[2]Shemyakin-Ovchinnikov Institute of Bioorganic Chemistry, Moscow 117997, Russia

[3]The Intellectual and Developmental Disabilities Research Center, The Semel Institute for Neuroscience and Human Behavior, and The Broad Stem Cell Research Center, The Jonsson Comprehensive Cancer Center, David Geffen School of Medicine at UCLA, Los Angeles, CA 90095, USA

[4]Research Institute for Future Medicine, Samsung Medical Center, Seoul 06351, Korea

[5]Department of Bioengineering, University of California, Los Angeles, Los Angeles, CA 90095, USA

[6]Jonsson Comprehensive Cancer Center, Broad Stem Cell Research Center, Brain Research Institute, University of California, Los Angeles, Los Angeles, CA 90095, USA

[7]Department of Neurosurgery, Ehime University, Japan

[8]Center for Precision Genome Editing and Genetic Technologies for Biomedicine, Federal Research and Clinical Center of Physical-Chemical Medicine of Federal Medical Biological Agency, Moscow, Russia

[9]Semel Institute for Neuroscience and Human Behavior, Departments of Psychiatry and Neurology, David Geffen School of Medicine, University of California, Los Angeles, CA, 90095, USA

[10]Department of Pharmaceutical Chemistry, University of California, San Francisco, San Francisco CA 94158, USA

[11]Center for Translational Neuromedicine, University of Rochester Medical Center, Rochester, NY, 14642, USA; and Faculty of Health and Medical Sciences, University of Copenhagen, Copenhagen 2200, Denmark

[12]Department of Cell, Developmental and Integrative Biology, University of Alabama at Birmingham, Birmingham, AL 35294 USA

[13]Department of Neurosurgery, Samsung Medical Center, Sungkyunkwan University School of Medicine, Seoul, Korea; Department of Health Science & Technology, Samsung Advanced Institute for Health Science & Technology, Sungkyunkwan University, Seoul, Korea.

[14]Research and Development Center for Precision Medicine, Tsukuba University 305-8550 Japan

[15*] Lead Contact

†These authors contributed equally to this work

***Correspondence:**

Ichiro Nakano, MD, PhD

Research and Development Center for Precision Medicine, Tsukuba University

1-2 Kasuga Tsukuba Ibaragi 305-8550

E-mail: nakano.ichiro.fw@u.tsukuba.ac.jp

Harley Kornblum, MD, PhD

Departments of Psychiatry, Pharmacology, and Pediatrics, David Geffen School of Medicine at UCLA, Los Angeles, CA 90095, USA

E-mail: hkornblum@mednet.ucla.edu

Key words: glioblastoma, vascular endothelial cells, endocan, ESM1, tumor heterogeneity

Running Title:

Vascular endothelial cell-controlled spatial identity for glioblastoma edge region

Abstract

Glioblastoma is a lethal brain cancer with active infiltration of tumor cells at the periphery where the vascular supply is enriched to create its own niche. Given that tumor recurrence is predominantly local, most of the seeds for lethal recurrence are hidden at the tumor edge and are surgically inaccessible. Here, we found that the spatial identity of the edge-located glioblastoma cells is, in the tested models, constructed by inter-cellular signals derived from the soluble factor endocan (protein product of *Esm1*) that is secreted by tumor-associated vascular endothelial (VE) cells. Injection of two distinct mouse glioblastoma models into *Esm1* knockout (KO) mice resulted in tumors that failed to form typical edge lesions, resulting in the formation of compact core-only lesions. In sharp contrast, tumors derived in WT (*Esm1*-intact) mice harbored both tumor core and edge structures. Despite these obvious phenotypic differences, the aggressiveness of these two tumor types was indistinguishable *in vivo.* Surprisingly, regardless of the host system, co-injection of mixture of these two tumor subpopulations gave rise tumors with much worse survival, indicating that the accumulating tumor cell heterogeneity contributes to elevate malignancy. Mechanistically, endocan competes with PDGF to bind and activate PDGFRα in human glioblastoma cells, accompanied with the upregulation of the *Myc* transcriptional activity *via* alterations in its promoter chromatin structure. One of the mainstays of glioblastoma treatment, radiation, induces endocan secretion from VE cells, which promotes the radioresistance of the edge-located glioblastoma cells, allowing for the persistence of the edge structure. Collectively, these data suggest that intra-tumoral spatial heterogeneity is initiated by the VE cell-derived endocan signals through PDGFRα to construct tumor edge-to-core (E-to-C) architecture to cause lethal tumor recurrence.

Introduction

Glioblastoma is a devastating intraparenchymal brain cancer with the hallmarks of peripheral hypervascularity and a high degree of intra-tumoral cellular and molecular heterogeneity. Surgical resection is limited in its curative potential due to the inability to completely eradicate tumor cells from the brain [1-3]. These post-surgical residual tumor cells are primarily located at the tumor edge (defined by the non-enhancing T2-FLAIR positive area on MRI, see **Figures 1A, S1A and B** for the definition of tumor edge). The unique ecosystem at the tumor edge is composed predominantly of functioning brain parenchymal cells with scattered tumor cells harboring rich vasculature. Thus, even with the ongoing attempt towards supra-total resection of glioblastomas designed to remove edge lesions in non-eloquent areas of the brain beyond the current standard core resection, the complete removal of tumor cells from the brain may not be a practically attainable goal. Subsequently, a majority of patients inevitably suffer from post-surgical lethal tumor recurrence with reconstruction of the tumor architecture with the core lesions [4-6]. Some of the residual edge-located tumor cells initiate this process, indicating that there is an edge-to-core (E-to-C) progression. In patient-derived pre-clinical glioblastoma models, this E-to-C phenotypic shift was observed particularly in tumor-initiating cells (TICs), and the E-to-C molecular signature was tightly associated with poorer prognosis of glioblastoma patients [4, 7]. We theorize that this E-to-C shift in post-surgical brains is a key determinant of tumor lethality.

Because of its accessibility, tumor core tissues (defined by the entire area within the Gadolinium-enhancing lesion on MRI; **Figures 1A, S1A and B**) likely represent the dominant source of the current molecular profiling studies (e.g. The Cancer Genome Atlas (TCGA) and Rembrandt). In recent years, however, several studies have started to gain molecular information about tumor cells at the edge located outside the area of contrast enhancement [8-10]. Likewise, through the collection of subcortical edge tissues from the non-eloquent deep

white matter during supra-total resection during awake procedures, we have molecularly characterized the edge- and core-located glioblastoma cells. Evaluation of their transcriptome, metabolome and kinome has revealed their distinctly-activated key molecules (e.g. Bruton's tyrosine kinase, Nitrogen metabolism) [5, 11, 12]. More importantly, their phenotypic differences have been revealed with the established tumor edge and core models derived from patient tumors, suggesting the presence of cell-intrinsic mechanisms for the spatial identities of individual tumor cells.

The tumor ecosystem is defined by cooperation and competition among different cell types within the tumor microenvironment. Recently, we identified two sets of intercellular signals associated with the spatially-distinct glioblastoma ecosystem: one derived from dying tumor cells providing growth-promoting and therapy-refractory signals to the near-by surviving tumors cells (most actively in the tumor core) [13] and the other from tumor core cells promoting radioresistance of their edge counterparts [5]. At the tumor edge, perivascular niches are a fertile environment for glioblastoma cells, including TICs, owing in part to the support of vascular endothelial (VE) cells [14, 15]. Various paracrine factors are provided by VE cells to maintain tumor-initiating properties and enhance therapy resistance of glioblastoma cells [14, 16-20]. Given that the tumor vasculature is predominantly enriched at tumor edge, we hypothesized that VE cell-driven signals contribute to create “edge-ness” and sought to determine factors elaborated by VE cells that could instruct tumor cells in their intra-tumoral spatial positioning. One of the factors that we identified in this study is endocan, a 20 kDa dermatan sulfate proteoglycan protein encoded by the *Esm1* gene [21]. Prior studies demonstrate that endocan is regulated by hypoxia/VEGF pathway and is a marker of endothelial cell activation, endothelial dysfunction during angiogenesis, and has been shown to be linked to tumor progression [22, 23]. The expression of endocan has been correlated with higher grade and shorter survival in glioma, and it has been notably detected in tumor margin [24]. However, the functional role of

138 endocan in glioblastoma remains unknown and therefore endocan has not been evaluated as a
139 therapeutic target even in experimental settings [24, 25].

140 In this study, we sought to uncover whether soluble factors including endocan from VE
141 cells have an instructive role in establishing the structural tumor heterogeneity, possibly
142 originating in the surgically-unresectable tumor edge, to then create the lethal tumor core
143 lesions in glioblastoma.

144

145

146 **Results**

147 **Tumor-associated VE cells promote glioblastoma aggressiveness in vivo, accompanied**
148 **by their secretion of endocan**

149 We first tested whether VE cells promote aggressiveness of glioblastomas in mouse brains by
150 using two VE cell models; one was a short-term primary culture with glioblastoma patient-
151 derived VE cells (TEC15) and the other was an immortalized brain VE cell line (HBEC-5i)
152 (**Figure S2B**). When these VE cells were co-injected with the patient-derived glioma sphere line
153 g1051x –a line that creates tumors in mouse brains harboring both core and edge phenotypes
154 [5] - at a 1:10 ratio into SCID mice, the survival of these mice was significantly shorter than the
155 control group in which g1051x was injected alone (**Figures 1B and S2C**).
156 Immunohistochemistry (IHC) of the co-injection group showed elevated expression of both
157 human and mouse CD31, indicating their possible conjoined role in promoting tumorigenesis in
158 these models (**Figure S2D**).

159 To identify potential trophic factors that could be elaborated by tumor-associated VE
160 cells, we isolated $CD31^+$ tumor-associated VE cells from 8 glioblastoma cases along with non-
161 cancerous $CD31^+$ cells from 5 craniotomies for epilepsy as controls. RNA-sequencing (RNA-
162 seq) analysis revealed *ESM1* (gene encoding the endocan protein) as the second most

significantly upregulated gene (FC=9.76, FDR-corrected *p*-value=0.0031) in tumor-derived CD31$^+$ cells compared to the non-neoplastic counterparts (**Figures 1C and 1D)**. In both TCGA and the Samsung Medical Center (SMC) brain tumor databases, *ESM1* expression was found to directly correlate with higher glioma grade, with significant elevation noted in Grade IV glioblastomas (**Figures 1E and 1F**). Survival analysis of glioma patients demonstrated that patients with high level of endocan protein had significantly shorter survival (**Figure 1G**). Given these clinical data, we then investigated whether endocan is secreted from VE cells. ELISA with CM from HBEC-5i cells, normal human astrocytes (NHA), and three glioma sphere lines (g157, g711, and g1051) exhibited significantly higher concentrations (>100pg/ml) of endocan exclusively secreted from HBEC-5i VE cell (**Figure 1H**). We further confirmed that tumor associated CD31$^+$ VE cells express endocan in the perivascular areas of our glioblastoma clinical samples detected by immunofluorescence (**Figure 1I**).

Endocan is required for establishing the hypervascular tumor edge structure in murine glioblastoma

We next investigated whether endocan plays a role in the establishment of the hypervascular tumor edge and/or core lesions. We utilized wild-type (WT) and *Esm1* knockout (*Esm1* KO) mice [26] as host systems for a tumor challenge. Of note, untreated *Esm1* KO mice did not have any apparent phenotype and the brain vasculature appeared to be normal (**Figure S3A**). We first used freshly-resected murine glioblastoma-like tumor cells isolated from tumors induced by RCAS-PDGAB injection into Nestin-Tva/Cdkn2a-/- mice [27]. Following dissociation into single cells, these murine tumors were then directly injected into the brains of WT and *Esm1* KO mice. The resultant tumors in WT mice (termed WTD tumors) exhibited numerous intra-tumoral hemorrhages in sharp contrast to grayish necrotic tumors in *Esm1* KO mice (*Esm1* KOD tumors) (**Figure 2A**). This difference was reflected by overtly fewer CD31$^+$ VE cells in *Esm1*

KOD tumors as compared to WTD tumors (**Figure 2B**). We then utilized another mouse glioblastoma model derived from mice harboring mutations in *p53*, *PTEN*, and *NF1*, termed as mg7080 [28]. *In vitro* glioma sphere cultures enriching for their TIC subpopulation [29] were established from these tumors (**Figure 2C**) and injected into WT and *Esm1* KO mice. IHC for CD31 also displayed a similar difference in vascularity, exhibiting hyper-vascular tumors in the WT animals and hypo-vascular tumors in the *Esm1* KO ones (**Figure 2D**)**.** At the ultrastructural level evaluated by electron microscopy, mg7080-derived WTD blood vessels exhibited an irregular basement membrane, typical of human glioblastoma, while the few blood vessels detected KOD tumors showed a more regular basement membrane (**Figure 2E**). Collectively, these data indicate that endocan secreted by VE cells instructs intratumoral vascular heterogeneity by creating vascular-rich tumor edge lesions.

Endocan-driven edge+core and endocan-depleted core lesions cooperatively increase intratumoral heterogeneity, elevating the malignancy of murine glioblastoma

Given the remarkable phenotypic difference in tumors with or without endocan in the host brain, we tested whether *Esm1* WTD and KOD cells maintain their phenotypes in the same brain microenvironment. Short-term mg7080 TIC-enriched sphere cultures from WT and KO mice were labeled with GFP- and mCherry-carrying lentivirus, respectively (**Figure 3A**). First, these tumor cells were intracranially co-injected into brains of WT BL/6 mice. IHC with anti-GFP and anti-mCherry antibodies demonstrated that the majority of mCherry-labeled KOD cells remained at the injection site, expanding to create characteristic tumor core lesions. In contrast, GFP-labeled WTD cells were widely distributed within the brain including the injection site (core lesion), as well as distant areas particularly in the corpus callosum and adjacent to the lateral ventricles, resembling the subcortical infiltrating pattern frequently seen in patients' glioblastomas (**Figure 3B, right panel**). This difference was unlikely due to differences in their

213 migration potential since the *in vitro* migration assay using patient derived GBM spheres with
214 and without endocan showed no noticeable difference by adding endocan into the culture
215 (**Figure S3B**). As expected, CD31 staining indicated that the core lesion predominantly formed
216 by KOD cells were hypovascular, while the edge lesion created mainly by WTD cells were
217 hypervascular (**Figures 3C and 3D**). These data suggest that KOD cells have lost their capacity
218 to develop the typical tumor edge structure even in the presence of endocan in the brain,
219 possibly due to lack of some receptor allowing for processing the response to endocan-driven
220 signals. In turn, when this co-injection was performed in *Esm1* KO mice, both GFP^+ WTD and
221 $mCherry^+$ KOD cells remained at or near the injection site, resulting in a compact tumor core
222 lesion without a typical infiltrative hypervascular edge, suggesting that even WTD cells can only
223 create the core lesion with a loss of the capacity to develop edge lesions – similar to the
224 phenotype of KOD tumor (**Figure 3E**). Surprisingly, the survival outcomes of these models
225 showed striking differences: despite the substantial difference in tumor vascularity and
226 localization, the survival of *Esm1* WTD and KOD single injection groups did not show any
227 noticeable difference irrespective of the host system (either WT or *Esm1* KO mice). In contrast,
228 the co-injection group exhibited significantly shorter survival when injected into both WT and
229 *Esm1* KO mice, despite their striking phenotypic differences in these genetically-distinct mouse
230 hosts (**Figures 3F and 3G**). Collectively, these data suggest that, as the ancestor-like tumor
231 subpopulation, endocan-dependent tumor cells harbor the capacity of forming tumor edge and
232 core lesions, giving rise to endocan-depleted tumor cells as their daughter-like progeny
233 population that have lost the capacity to establish edge lesions. However, regardless of the
234 endocan status in the host, these two tumor subpopulations evolve to establish more
235 aggressive, heterogeneous tumors.
236
237 **Endocan binds to and phosphorylates PDGFRα in human glioblastoma cells**

Next, we sought to identify the receptor for endocan in glioblastoma cells. We first purified proteins from the plasma membrane of the well-characterized human glioma sphere line g157 [30] and incubated these proteins with immobilized endocan. Subsequent elution of bound proteins followed by mass spectrometry unexpectedly identified PDGFRα as a potential endocan-interacting protein (**Figure 4A**). To confirm these data in a cell-free system, we tested the interaction of the corresponding recombinant proteins. Immunoprecipitation experiments demonstrated physical interaction between F_c-tagged PDGFRα and His-tagged endocan (**Figure 4B)**. As another validation, we used the proximal ligation assay, which showed that rhEndocan induces the dimerization of PDGFRα, indicating that endocan is capable of inducing the initial step in PDGFRα activation [31-33] (**Figure S4A**). To further examine the specificity and binding affinity of endocan's interaction with PDGFRα, we performed a binding competition assay between endocan and PDGFBB, a known major ligand for PDGFRα, labeled with Alexa488 and Alexa647 fluorescent dyes, respectively. rhPDGFBB diminished rhEndocan binding to glioblastoma cells in a concentration-dependent manner; similar data were obtained in the opposite experiment where rhEndocan decreased rhPDGFBB binding. Importantly, we observed that rhEndocan at a 10ug/ml concentration was able to completely displace rhPDGFBB from glioblastoma cells, while rhPDGFBB at the corresponding concentration was able to displace only half of the rhEndocan molecules present (**Figures 4C, and S4B**). Consistent with these data, gene set enrichment analysis (GSEA) of the RNA-seq data with mg7080-derived tumors demonstrated that *Esm1* KOD tumors exhibited downregulation of PDGF-mediated signaling pathway and diminished PI3K/AKT signaling network compared to WTD tumors, suggesting the possibility of cell survival conferred by endocan through PDGF-driven pathways (**Figures S4C and Table S1**). As expected, various vasculature-associated genes (e.g. *PODXL* (podocalyxin), *PECAM1* (Platelet Endothelial Cell Adhesion Molecule), *ACTA2* (Smooth Muscle Actin), *VWF* (Von Willebrand Factor), CLDN*5* (claudin 5)) were also

significantly reduced in KOD tumors as compared to WTD ones (**Figure S4D**). Consistent with these experimental data, IHC of patient glioblastomas displayed the presence of endocan^{+} cells within perivascular areas of tumors that are adjacent to PDGFRα^{+} cells (**Figure 4D**).

Given that downstream activation through PDGFRα requires receptor autophosphorylation, we further investigated whether the addition of recombinant endocan alters the phosphorylation levels of PDGFRα in glioma spheres *in vitro*; PDGFBB was used as a positive control [34]. In this experiment, g1079 cells were treated with rhEndocan or rhPDGFBB, and phosphorylation of PDGFRα at Y720 was measured by western blotting at different time points. rhEndocan (10 ng/ml) induced appreciable phosphorylation of PDGFRα as early as 15 minutes after addition and displayed similar temporal kinetics to that of PDGFBB (**Figure 4E**). rhEndocan treatment also resulted in the phosphorylation of the PDGFRα downstream targets p85α, PI3K, and GSK-3β, further confirming activation of this signaling interaction, along with phosphorylation activities of p-GSK3β and p44/42 MAPK (**Figure 4F**).

Given that PDGFRα is a key regulator of glioblastoma aggressiveness and that endocan may function as a gatekeeper to turn on this signaling [35-37], we next investigated whether the elimination of PDGFRα activation produces distinct effects in *Esm1* WT and KO background. We hypothesized that blockade of PDGFRα signaling in the *Esm1* WT background would prevent the formation of endocan-induced tumor edge lesions. To this end, we treated *Esm1* WT and KO mice bearing mg7080−derived tumors with Ponatinib, a kinase inhibitor with relatively high selectivity toward PDGFRα [38]. Ponatinib enhanced the survival only of the tumor-bearing WT, but not *Esm1* KO mice (**Figure 4G**). As indicated by immunostaining with WTD tumors, the treatment resulted in a loss of Myc and Olig2 (both markers associated with tumor edge cells) **(Figure 4H)**. On the other hand, we observed increased expression of p65-NFkB (a marker associated with tumor core cells)（**Figure 4H)**. These results suggest that, in

this particular tumor model, the PDGFRα-driven glioblastoma growth *in vivo* is mediated by endocan.

Endocan-mediated signaling alters chromatin accessibility in glioblastoma cells, including the promoter region of the Myc gene

Given the persistence of edge- and core-related phenotypes even following removal from the brain, we hypothesized that the endocan-PDGFRα signaling could modify some chromatin structure to retain long-term intratumoral spatial identity. To test this possibility, we performed ATAC-seq (Assay for Transposase-Accessible Chromatin sequencing) with *Esm1* WTD and KOD to assess whether and how endocan affects chromatin accessibility [39]. In fact, alterations in chromatin structure were noticeably very focused with only 10 genes identified with significantly different chromatin accessibility in their promoter regions among these tumors (**Figures 5A and Table S2**). To explore the relationship between open chromatin and gene expression levels, we next performed RNA-seq analysis on the same samples and compared the gene expression levels by RNA-seq with the promoter accessibility data by ATAC-seq (**Figures 5B and 5C and Table S3**). Our results highlighted that the *Myc* gene - a downstream target of PDGFRα pathway [40]- was among the few genes with both increased promoter accessibility (open chromatin) and upregulated expression in WTD tumors compared to KOD tumors. In addition, IHC of mg7080 tumors showed higher expression of cMyc in WTD tumors as compared to *Esm1* KOD ones (**Figure 5D**). Taken together, these data suggest that, similar to PDGFRα, endocan regulates the open state of the chromatin structure for the *Myc* promoter region, thereby activating its transcription (**Schema in Figure 5E**).

Endocan protects edge-located glioblastoma cells from radiotherapy-induced cell death *in vivo*

We next sought to determine whether standard glioblastoma treatments of radiation and temozolomide (TMZ) influences endocan production or effects. While both radiation and TMZ induced an elevation of *ESM1* mRNA *in vitro* as measured by qRT-PCR (**Figure S5A and S5B**), a more pronounced elevation of endocan protein was observed in radiated HBEC-5i cells as determined by ELISA (**Figure 6A**). Given these findings, we then investigated whether endocan secreted by VE cells plays a role in radioprotection in glioblastoma cells. We pretreated four patient-derived glioma sphere lines (g157, g711, g1051 and g1079) with rhEndocan (10ng/ml) for 3 days, followed by radiation treatment at 8 and 20 Gy. Analysis of these glioma spheres on day 5 post-irradiation determined that rhEndocan pretreatment significantly enhanced cell growth in three cell lines (**Figure 6B**), and decreased radiation-induced induction of caspase 3/7 activity assay even at radiation dose as high as 20 Gy (**Figures S5C, S5D)**. These effects were at least partially attenuated by treatment of cells with a blocking antibody for endocan (**Figure 6C**).

We then created two tumor models by transplanting either WTD or KOD tumor cells into WT brains, followed by treatment with an 8 Gy dose of radiation. Both tumor models showed substantial shrinkage in size after radiation; nonetheless, the location of the resultant tumor cells and the subsequent survival benefit were clearly different. Following radiation, residual KOD tumor cells were scattered randomly around the injection sites, whereas post-radiation WTD cells predominantly resided in the most distant areas in the corpus callosum - the "far-edge area" and one of the most frequent brain regions with glioblastoma recurrence after treatment failure [41, 42] . Subsequently, radiation showed a significantly greater effect on the survival of tumor-bearing KO mice than in WT mice (**Figure 6D and 6E**). These data suggested that endogenous endocan protects the tumor cells from radiation damage, thus promoting tumor growth and diminishing animal survival.

Finally, we performed RNA-seq with glioma spheres that were treated with either HBEC-5i CM or rhEndocan in presence of 8 Gy of radiation dose. Bioinformatics analysis demonstrated that both HBEC-5i CM and endocan induce pronounced alterations in gene expression, and importantly, addition of rhEndocan largely recapitulated the effects of HBEC-5i CM on post-irradiation glioma spheres (**Figure 6F**). In fact, there was more than 70% concordance of genes whose level of expression was altered more than 2-fold by both treatments. These findings suggest that rhEndocan is one, if not the only, major mediator for the VE cell-driven radioprotective effect on glioblastoma cells.

Discussion

Biological mechanisms of tumor evolution in primary glioblastoma cannot be directly investigated in humans. With murine tumor models, this study uncovered that the cellular hierarchy between two cell types that progress from a bi-potent edge+core-forming cell to core-restricted mono-potent cells, no longer capable of producing cells capable of establishing typical edge lesions. Unexpectedly, this cellular hierarchy is driven by a soluble factor from VE cells, endocan. In the tumor microenvironment, this lineage-commitment occurs not only by depletion of endocan (e.g. WTD cells in KO mice), but also loss of the ability to respond to endocan, e.g. a receptor, in tumor cells (e.g. KOD cells in WT mice). We identified PDGFRα as a critical receptor for endocan. Given the major roles of PDGFRα signaling in the propagation of glioblastoma and other cancers, this data opens up new avenues of studying this endocan-PDGFRα signaling axis [35, 43]. A critical question is how much of the effect of endocan on tumor growth, radioprotection, and creation of the edge phenotype is due to the PDGFRα-dependent signaling and how much is due to other mechanisms (**Illustration shown in Figure 7**). Our observations with ponatinib suggest that signaling through PDGFRα does play a

dominant role on endocan effect but does not exclude the possibility that endocan also acts through undetermined PDGFRα-independent pathways. Given that hypovascular tumors in *Esm1* KO mice would presumably retain PDGFBB or other PDGFs in the microenvironment, endocan and PDGFs might drive sufficiently different downstream signaling cascades to create different phenotypic outcomes. Another possibility is that PDGF ligand concentrations are simply insufficient to fully activate the overlapping downstream signaling, subsequently causing the less heterogeneous tumor phenotype.

Despite the striking phenotypic difference of the WTD and KOD tumors, the secondarily generated core-located cells following endocan depletion were not solely a differentiated progeny. It is reasonable to expect that the edge+core-generating ancestor-like cells should be more malignant as opposed to the differentiated core-restricted progeny cells; nonetheless, the survival of mice bearing WTD and KOD tumors are comparably similar. To our surprise, when these two were combined, the resultant tumors displayed elevated malignancy, killing mice faster than either alone. Of note, the WTD and co-injected tumors were phenotypically quite similar, harboring both tumor edge and core. Collectively, these findings suggest that WTD and KOD cells combine to extend the cellular heterogeneity in co-injected tumors, possibly through a reflection of a cellular evolution mechanism. Taking the date this murine tumor model together, we observed two sets of data that can only be explained by referring to both of two different mechanisms: the cellular hierarchy theory (ancestor-like cells producing more fate-restricted daughter cells) and the cellular evolution theory (two subtypes of tumor cells independently contribute to tumor malignancy). From the therapeutic stand-point, our findings indicate that surgery will need to eradicate the core cells completely, and that post-surgical adjuvant therapies should then focus on the control of the edge cells toward achieving either elimination or dormancy, preventing them from propagating and evolving into core lesions. Further studies with multiple different preclinical models, possibly with patient-derived ones, are warranted.

Tumors are composed of two distinct subpopulations including the one that is located at tumor edge, endocan-responsive, and more radioresistant [5]. Given the clinical challenges that would be involved in the complete resection of edge-located tumor cells, the identification of therapeutic targets associated with the tumor edge are an urgent need. Since a global KO of *Esm1* does not cause noticeable defect in the brain or other organs, the idea of systemically diminishing, or even completely eliminating, tumor-associated and/or radiotherapy-induced endocan to control glioblastoma recurrence seems to be promising [26]. Furthermore, endocan's vascular origin indicates that the blood brain barrier may not be a major roadblock to the development of such therapeutics. However, single target approaches have failed for years to control therapy-refractory cancers like glioblastoma. It is likely that future treatment strategy would require the eradication of both endocan-responsive edge-located cells as well as their endocan-independent core-located progeny as combination.

ACKNOWLEDGEMENTS

We would like to express our sincere appreciation to all the patients and families, who kindly allowed us to obtain their tumor samples for this study. We thank Dr. Ralf Adams (Max Planck Institute for Molecular Biomedicine) for generously sharing cryopreserved *Esm1* embryos. We would also thank all our collaborating scientists, as well as the assigned reviewers and Editor for this manuscript, for the constructive comments and suggestions. Lastly, we acknowledge the contribution by all the members in the Nakano and Kornblum laboratories (past and present) for technical assistance.

FUNDING

This work was supported by NIH grants R01NS083767, R01NS087913, R01CA183991, R01CA201402 (I.N.), R01NS104339 (A.B.H), NS052563 (H.I.K.) the UCLA SPORE in Brain Cancer, P50 CA211015 (H.I.K.); by the Russian Foundation for Basic Research grants 17-29-06056 (M.S.P.), 17-00-00172 (K.S.A.), 20-04-00804 (M.S.P.) and 20-34-70147 (M.S.P.); Russian Science Foundation grant 19-44-02027 (M.S.P.); grant 075-15-2019-1669 from the Ministry of Science and Higher Education of the Russian Federation (K.S.A.) and the Dr. Miriam and Sheldon G. Adelson Medical Research Foundation (H.I.K., A.L.B., S.A.G). D.N was supported by the Korea Health Technology R&D Project through the Korea Health Industry Development Institute (KHDI), funded by the Ministry of Health and Welfare, Republic of Korea (HI4C3418).

AUTHOR CONTRIBUTIONS

Leading conceptualization: I.N; Critical rationalization: S.B, M.S.P, H.I.K, I.N; Methodology: S.B, M.S.P, A.B.H, H.I.K, I.N; Laboratory investigation: S.B, M.S.P, Y.G, S.D.M, D.Y, M.S.K, J.A.O, B.T, A.L.B, A.S, S.K.S; Bioinformatics analysis: H.J.C, Y.L, K.S.A, R.K, Y.C; Writing - Original Draft: S.B, I.N; Writing – Review & Editing, S.B, M.S.P, H.I.K, I.N; Funding Acquisition: M.S.P, K.S.A, A.B.H, H.I.K, A.L.B, S.A.G, I.N; Resources: H.I.K, A.L.B, I.N; Supervision: H.I.K, I.N. All authors had substantial input to the logistics of the work and revised and approved the final manuscript. The authors know their accountability for all aspects of the study ensuring that questions regarding the accuracy and integrity of any part are appropriately investigated and resolved. The corresponding authors had full access to all the data and the final responsibility to submit the publication.

DISCLOSURES

The authors have nothing to disclose.

METHODS

Informed consent and ethics committee approvals. This study was conducted under protocols approved by the IRBs and IACUCs of University of California Los Angeles (UCLA), MD Anderson Cancer Center (MDA), and University of Alabama at Birmingham (UAB).

The following experimental procedures were reported in our recent papers in detail [5, 11, 13].

Human Glioma sphere cell cultures. As described previously, glioma sphere cultures were maintained in DMEM/F12 medium supplemented with 2% B27 supplement (% vol), 20 ng/ml bFGF, and 20 ng/ml EGF. The bFGF and EGF reagents were added twice a week, and the culture medium was replaced every 7 days. Experiments with neurospheres were performed with lines that were cultured for fewer than 30 passages since their initial establishment. STR analysis was performed to confirm cell identity. The cell lines tested negative for mycoplasma contamination.

Human Tumor-Associated Endothelial Cell culture. Glioblastoma tissues from patients were freshly isolated during surgery, manually dissociated into single cells, and these cells were sorted for CD31+ cells using magnetic beads (ThermoFisher Scientific). Following confirmation of CD31 expression, VE cells were grown in fibronectin-coated flasks with 2% FBS, 1% Penicillin-Streptomycin solution and 40µg/ml Endothelial growth supplement. Expression of CD31 was periodically checked by flow cytometry.

Murine Glioma sphere cell cultures. Spontaneous tumors formed in *PTEN*, *TP53*, *NF1* deleted mice [44] were grown in neurosphere media as described previously (mG7080).

Freshly obtained mouse tumor in Fig 2A. Freshly obtained mice tumor was kindly shared by Dolores Hambardzyuman lab (Emory University). Tumor bearing hemisphere was visualized and tumor was isolated to obtain single cells for injection into mice.

HBEC-5i (ATCC) cells: These cells were cultivated in DMEM/F12 medium containing 10% FBS, 1% Penicillin-Streptomycin solution and 40µg/ml Endothelial cell growth supplement.

Genetically modified mice. *Esm1* KO (Bl/6) mice are a generous gift from Dr. Ralf H. Adams[26]. All animals were maintained in accordance with the National Institute of Health (NIH) Guide for the care and Use of Laboratory Animals and were handled according to protocols approved by the University of Alabama at Birmingham subcommittee on animal care (Institutional Animal Care and Use Committee). Genomic status of *Esm1* was periodically confirmed by PCR according to the prior studies [26].

In Vivo Intracranial Xenograft Tumor Models. As described previously, 6-8-week-old NOD SCID mice ($Prkdc^{scid}$) were used for intracranial tumor formation. In each mouse, 5 x 10^5 cells of human patient-derived glioblastoma cells were injected intracranially into groups of 6-8-week-old mice. Detailed protocol is described elsewhere [13].

***In Vivo* Syngeneic Intracranial Tumor Models.** Our general protocol for the intracranial tumor models was described previously [13]. Briefly, 0.5 million murine glioblastoma cells were injected into the brains of Bl/6 or *Esm1* KO mice as previously described [5]. Mice were monitored and sacrificed when neuropathological symptoms developed. For immunohistochemical studies, mice were perfused with ice-cold PBS, followed by 4% paraformaldehyde (PFA). Mice brains were dissected and fixed in 4 % PFA solution for 48 hours and then transferred to 10% formalin for 48 hours. For tumor collection for RNA extraction, mice were sacrificed, and tumors were isolated and fast-frozen using liquid nitrogen.

***In vivo* drug treatments.** Mice were injected with mg7080 tumors to form intracranial tumors. On day 14 post injection, mice were treated with 50mg/kg/day of Ponatinib as recommended by manufacturer's protocol (Selleckchem). Mice were administered ponatinib via oral gavage.

Endocan enzyme-linked immunosorbent assay (ELISA). The concentration of secreted Endocan was measured using the Endocan ELISA kit (Boster Bio) according to the manufacturer's protocol. Briefly, conditioned media was collected from the cells as mentioned and used for the experimental study.

Protein labeling. Recombinant Endocan and PDGFBB were labeled with Alexa Fluor 488 Microscale Protein Labeling Kit and Alexa Fluor™ 647 Microscale Protein Labeling Kit respectively. Labeled proteins were added to glioblastoma cells in different concentrations and after 30 min incubation on ice, cells were washed twice with PBS and analyzed by Attune NxT Flow Cytometer (Thermofisher Scientific). The obtained data were processed with FlowJo 10 software.

Proximal Ligation Assay. Glioblastoma cells were plated in wells of Lab-Tek II chamber pre-coated with laminin and treated with Endocan or PDGFBB for 90 minutes. Next, cells were washed 3 times with phosphate-buffered saline (PBS) and fixed with 4% PFA in PBS for 15 min at room temperature. Cells were washed 2 times with PBS and permeabilized with 0.2% Triton-X100 in PBS for 15 minutes. All subsequent procedures were performed using "Duolink In Situ Orange Starter Kit" (Duolink) according to the manufacturer's protocol.

Recombinant protein pull-down assay. To obtain a protein complex, recombinant His-tagged Endocan (R&D) was immobilized on 50 µl of HisPur Ni-NTA Magnetic Beads (Thermo Fisher Scientific) according to the manufacturer's protocol. The beads were washed 3 times with PBS and incubated for 2 hours with Fc-tagged recombinant PDGFRa (R&D) under constant

agitation. Next, beads were washed 3 times with PBS and bounded proteins were eluted with 300 mM imidazole in PBS and subjected to subsequent western blot analysis.

Mass spectrometry. Recombinant His-tagged Endocan (R&D) was immobilized on 50 µl of HisPur Ni-NTA Magnetic Beads (Thermo Fisher Scientific) according to the manufacturer's protocol. The beads were washed 3 times with PBS and incubated with fraction of plasma membrane proteins that were isolated from g1079 cells as described previously[45] and solubilized in lysis buffer (50 mM Tris-HCl, 150 mM NaCl, 1% Triton X100, 0.1% sodium deoxycholate, protease inhibitor cocktail, pH 7.5). Next, beads were washed once with lysis buffer and 3 times with PBS and bounded proteins were eluted with buffer containing 8M Urea, 2M Thiourea, 10 mM Tris (pH=8). Protein concentrations were determined using the QuickStart Bradford protein assay (Bio-Rad) according to the manufacturer's protocol. Then protein disulfide bonds were reduced with 5 mm DTT at RT for 30 min and afterward alkylated with 10 mm iodoacetamide at room temperature for 20 min in the dark. Detailed protocol can be found in previous publication [13].

In vitro migration experiment. Glioma cells were cultured and dissociated into single spheres. They were encapsulated with hydrogels as described in previous study [46].

Exogenous Immunoprecipitation Assay. Recombinant PDGFRα and Endocan (R&D) were mixed together and incubated with pre-washed magnetic beads and volume was adjusted to 500 µL with Lysis Buffer and incubated with mixing under 4°C for 1 h to remove unspecific bindings. The supernatant was collected with a magnetic stand and then incubated with the antibody and mixed under 4°C overnight. Antigen sample/antibody mixture was transferred to the tube and incubated with mixing under room temperature for 1 h. Magnetic beads were collected with a magnetic stand and incubated with low-pH elution buffer at room temperature with mixing for 10 min. The beads were magnetically separated and supernatant containing

target protein was saved. The pH was normalized with 15 µL of neutralization buffer for each 100 µL of elution buffer. IP samples were then loaded for electrophoresis with 4%-12% Bis-Tris protein gel.

Transmission Electron microscopy. Tissue from tumor-bearing mice were resected after anesthetizing, perfusing with 1X PBS. Tissue was immediately fixed in 2% glutaraldehyde at RT (1 hour). The brains were then dehydrated in different concentrations of ethanol and 1% uranyl acetate in 50% ethanol. Samples were then embedded and visualized using Tecnai Spirit T12 Transmission Electron Microscope.

ATAC sequencing and analysis. Previously-described methods [39] were used to perform ATAC-sequencing. Briefly, 50,000 cells were washed with 50mL ice cold PBS and re-suspended in 50mL lysis buffer (10 mM Tris-HCl pH 7.4, 10 mM NaCl, 3 mM MgCl2,0.2% (v/v) IGEPAL CA-630). The suspension was centrifuged at 500g for 10 minutes at 4 degrees. Samples were added with 50mL trans-position reaction mix of Nextera DNA library preparation kit (FC-121-1031, Illumina). Samples were amplified by PCR and incubated at 37C for 30 minutes. MinElute Lit (Qiagen) was used to isolate DNA. NextSeq 500 High Output Kit v2 (150 cycle, FC-404-2002, Illumina) was used to sequence ATAC library. For analysis, alignment was carried out using the Burrows-Wheeler Aligner mem, peak calling using MACS2 (with parameter setting –nomodel –shift 75), GO enrichment analysis and peak annotation using HOMER.

RNA sequencing. cDNA were used in the library preparation using Ovation® Ultralow Library Systems (NuGEN) and samples were sequenced using an Illumina HiSeq 2000 sequencer (Illumina, San Diego, CA) in high output mode across 9 lanes of 50bppaired-end sequencing, corresponding to 4.3 samples per lane and yielding between ~45 million reads per sample. Additional QC was performed after the alignment to examine the level of mismatch rate, mapping rate to the whole genome, repeats, chromosomes, key transcriptomic regions (exons,

introns, UTRs, genes), insert sizes, AT/GC dropout, transcript coverage and GC bias. Outliers were removed based on QC results. Between 60 and 82% (avg 76%) of the reads were mapped uniquely to the human genome. Total counts of read-fragments that were aligned to all the candidate gene regions were derived using HTSeq program (www.huber.embl.de/users/anders/HTSeq/doc/overview.html) with Human Hg38 (Dec.2014) RefSeq (refFlat table) as a reference and used as a basis for the quantification of gene expression. Only uniquely mapped reads were used for subsequent analyses. Differential expression analysis was conducted with R-project and the Bioconductor package edgeR. Statistical significance of the differential expression, expressed as Log_2 Fold Change (logFC), was determined, using tag-wise dispersion estimation, at p-Value of <0.005 unless stated otherwise. FPKM values were reported as a measure of relative expression units.

Flow cytometry. For CD44 staining glioma spheres were dissociated into single cells and stained with anti-CD44-APC antibody (Miltenyi Biotec) according to manufacturer's protocol. For CD133 staining, glioma spheres were dissociated into single cells and stained with anti-CD133-FITC (Biolegend) according to manufacturer's protocol. For apoptosis assay, cells were stained with CellEvent Caspase-3/7 Green Flow Cytometry Assay Kit (ThermoFisher Scientific) according to the manufacturer's protocol. All samples were analyzed by Attune NxT Flow Cytometer (Thermofisher Scientific) and the data were processed with FlowJo 10 software.

Cell count assay. AlamarBlue reagent (Thermo Scientific) was used to determine the cell number under various treatments. Briefly, cells were seeded at a density of 5,000 cells per well in 96-well plates. AlamarBlue reagent was added into each well and fluorescence was measured (Excitation 515-565 nm, Emission 570-610 nm) using Synergy HTX multi-mode reader (BioTek).

Western blot. The cell lysates were prepared in RIPA buffer containing 1% protease and 1% phosphatase inhibitor cocktail on ice. The sample protein concentrations were determined using the Bradford method. Equal amounts of protein lysates (10 µg/lane) were fractionated on a NuPAGE Novex 4%–12% Bis-Tris Protein Gel (Thermo Fisher Scientific) and transferred onto a PVDF membrane (Invitrogen, Thermo Fisher Scientific). Subsequently, the membranes were blocked with 5% skim milk or 5% BSA for 1 hour and then treated with the appropriate antibody at 4°C overnight. Protein expression was visualized with an Amersham ECL Western Blot System (GE Healthcare Life Sciences). β-Actin served as a loading control. ImageJ software (NIH) was used to analyze the Western blot results.

Immunohistofluorescence. Immunohistofluorescence (ICF) method was described previously [5]. Briefly, tumors embedded in paraffin blocks were deparaffinized using Xylene and hydrated through 100%, 95% and 75% ethanol gradient. Antigen was retrieved using DakoCytomation target retrieval solution pH 6 (Dako). These samples were then blocked with serum-free protein block solution (Dako) and incubated with corresponding primary antibodies at 4°C overnight. Next, slides were incubated with Alexa Flour-conjugated secondary antibody for 1 hr at room temperature and mounted in Vectashield mounting medium containing DAPI (Vector Laboratories). Nikon A1 Confocal microscope (Nikon) was used to capture images.

Immunohistochemistry. Immunohistochemistry (IHC) method was described previously (Wang et al., 2017). Briefly, tumors embedded in paraffin blocks were deparaffinized using Xylene and hydrated through 100%, 95%, and 75% gradient of ethanol. Slides were then microwaved in the presence of DakoCytomation target retrieval solution pH 6 (Dako). Slides were incubated with 0.3% hydrogen peroxide solution in methanol for 15 minutes at room temperature to inhibit internal peroxide activity. Slides were then blocked with serum-free block solution (Dako) and incubated with corresponding primary antibody overnight at 4°C. Next, samples were incubated

with EnVision+ System-HRP labeled Polymer (Dako) and visualized with DAB peroxidase substrate kit (Vector Laboratories). IHC scoring was performed using a previously described method (Klein et al., 2001). Samples with scores more than 4 were considered as "high" expression group. Images were captured using Nikon EVOS® FL inverted microscope (Nikon).

Lentivirus production and transduction. 293FT (Invitrogen) cells were co-transfected with vector encoding the GFP(Addgene) or mCherry (Addgene) using calcium phosphate (Clontech) for lentivirus production. Lentivirus was harvested at 72 hr after transfection and concentrated 100-fold using Lenti-X concentrator (Clontech). Infection of lentivirus was performed according to the manufacturer's protocol.

Tissue Microarray. Tissue microarray consisting of 0.6-mm cores from formalin-fixed, paraffin-embedded tissue blocks were generated using patient derived glioblastoma tissue samples at the Osaka City University.

RNA Isolation and Quantitative Real-time PCR. mRNA was extracted and purified using the Qiagen RNeasy Mini kit according to the manufacturer's protocol. Nanodrop 2000 spectrophotometer was used to determine the concentration and quality of RNA. RNA (0.5-1µg) was reverse-transcribed in cDNA using iScript reverse transcription supermix (Bio-Rad) that was then amplified using the following cycling conditions. Cycling conditions were 95°C for 5 min, and then 50 cycles of 95°C for 30 s, 60°C for 30 s and 72°C for 30 s. qRTPCR was performed on StepOnePlus thermal cycler (Thermo scientific) with SYBR Select Master Mix (Thermo Scientific). 18s, Bactin or GAPDH were used as an internal control.

Quantification and Statistical analysis. All data are expressed as the mean ± SD. *P* values were calculated in Graph Pad Prism 8.0 using a two-tailed Student t test which can be found in the individual figures and figure legends. *P* values less than 0.05 were considered to be

significant. Log-rank analysis was used to determine the statistical significance of Kaplan-Meier survival curves, and no samples, mice or data points were excluded from the analysis reported in this study. Unless otherwise noted, statistical analysis was performed by Prism 6 (Graphpad Software).

Data availability. All raw RNA-seq data will be available in the NCBI Gene Expression Omnibus (prepared prior to publication).

Reagent list.

REAGENT or RESOURCE	SOURCE	IDENTIFIER
Antibodies		
Anti-ALDH1A3	Sigma-Aldrich	Cat# SAB1300933, RRID:AB_10607145
Anti-phospho AKT (Ser473)	Cell Signaling Technology	Cat# 9271, RRID:AB_329825
Anti-AKT	Cell Signaling Technology	Cat# 9272, RRID:AB_329827
Anti-β-ACTIN	Cell Signaling Technology	Cat# 2118; RRID:AB_561053
Anti-CD133-APC	Miltenyi Biotec	Cat# 130-090-826; RRID: AB_244340
Anti-CD31	Abcam	Cat# ab28364, RRID:AB_726362
Anti-CD31	Novus	Cat#NB600-562, RRID:AB_10002476
Anti-CD44	Cell Signaling Technology	Cat# 3578; RRID: AB_2076463
Anti-CD44-FITC	BioLegend	Cat# 338804, RRID:AB_1501197
Endocan blocking antibody	R&D systems	Cat# AF1810-SP
Anti-ESM1	Abcam	Cat# ab56914, RRID:AB_941479
Anti-ESM1	Bioss	Cat# bs-3615R, RRID:AB_10857499
GAPDH	Abcam	Cat# ab9483; RRID: AB_307273
Anti-Goat IgG control	Thermofisher Scientific	**Catalog #** 02-6202
Anti-GFP	Abcam	Cat# ab290; RRID:AB_303395
Anti-phospho GSK3β (Thr 390)	Bioss	Cat# bs-3148R, RRID:AB_10857056
Anti-GSK3β	Cell Signaling Technology	Cat# 12456, RRID:AB_2636978
Anti-HIF1α	Novus	Cat# NB100-105, RRID:AB_10001154
Anti-His-tag	Cell Signaling Technology	Cat# 12698, RRID:AB_2744546
Rabbit IgG Isotype Control	Thermofisher Scientific	Cat# 02-6102, RRID:AB_2532938
Anti-phospho-p44/42 MAPK	Cell Signaling Technology	Cat# 9101, RRID:AB_331646
Anti-p44/42 MAPK	Cell Signaling Technology	Cat# 9102, RRID:AB_330744

Anti-mCHERRY	Novus	Cat# NBP2-25157, RRID:AB_2753204
Anti-MYC	Santa Cruz Biotechnology	Cat# SC-40; RRID: AB_627268
Anti-p65-NF-κB(pS536)	Abcam	Cat# ab86299, RRID:AB_1925243
Anti-OLIG2	Millipore	Cat# AB9610; RRID: AB_570666
Anti-PI3K p85 / p55, phospho (Tyr199)	Bioworld Technology	Cat# BS4605, RRID: AB_1663852
Anti-PI3K	Cell Signaling Technology	Cat# 4292, RRID:AB_329869
Anti-phospho PDGFRα (y720)	Abcam	Cat# ab134068
Anti-PDGFRα	Cell Signaling Technology	Cat# 3174, RRID:AB_2162345
Anti-PDGFRα (C-terminal)	Sigma-Aldrich	Cat# SAB1404186, RRID:AB_10737660
Bacterial and Virus Strains		
E. coli Stbl3 Competent cells	ThermoFisher	Cat# C737303
Biological Samples		
Human glioma tissue microarray	This study	N/A
Human glioma tissues	This study	N/A
Human blood plasma samples	This study	N/A
Mouse tissues	This study	N/A
Chemicals, Peptides, and Recombinant Proteins		
EGF	Peprotech	Cat# AF-100-15
bFGF	Peprotech	Cat# AF-100-18B
B27	Thermofisher	Cat# 12587010
Heparin	Sigma	Cat# H3149
DMEM/F12	Thermofisher	Cat# 10565-018
StemPro Accutase	Thermofisher	Cat# A1110501
Fetal bovine serum	Thermofisher	Cat# 10438018
Penicillin-Streptomycin	Thermofisher	Cat# 15140122
Laminin	Sigma	Cat# 11243217001
Endothelial cell growth supplement	Sigma	Cat# E2759
RIPA buffer	Sigma	Cat# R0278
Phosphatase inhibitor cocktail	Sigma	Cat# P2850
Protease inhibitor cocktail	Sigma	Cat# P8340
Blotting Grade Blocker Non Fat Dry Milk	Bio-Rad	Cat# 1706404XTU
iScript reverse transcription supermix	Bio-Rad	Cat# 1708841
SYBR select master mix	Thermofisher	Cat# 4472918
Serum-free protein block solution	Dako	Cat# X090930-2
Vectashield mounting medium containing DAPI	Dako	Cat# H-1200
DakoCytomation target retrieval solution pH6	Dako	Cat# S236984-2

Envision+ System-HRP labeled Polymer	Dako	Cat# K400211-2
AlamarBlue reagent	ThermoFisher	Cat# DAL1100
Alexa-Fluor 488 5-TFP Ester	ThermoFisher	Cat# A30005
Polybrene	EMD Millipore	Cat# TR-1003-G
Puromycin	Sigma	Cat# P7255
Recombinant Endocan	R&D	Cat#
Recombinant PDGFBB	R&D	
Alexa-Fluor 647 microscale protein kit	Thermofisher	Cat# A30009
Duolink Insitu Orange Starter Kit	Duolink	Cat# DUO92102
HisPur Ni-NTA Magnetic Beads	Thermofisher	Cat# 88831
F_c Tagged recombinant PDGFRα		Cat# 6765-PR-050
Critical Commercial Assays		
Dual reporter luciferase assay	Promega	Cat# E1910
HiSpeed Plasmid Midi RNeasy mini kit	Qiagen	Cat# 12643
Kit miRNeasy mini kit	Qiagen	Cat# 217004
Qiagen Cat# 74104 DAB peroxidase substrate kit	Vector Laboratories	Cat# SK-4100
CellEvent Caspase-3/7 Green Flow Cytometry Assay Kit	ThermoFisher	Cat# C10427
Autophagy Detection Kit	Abcam	Cat# ab139484
Quick Start Bradford protein assay	Bio-Rad	Cat# 5000201
TruSeq Stranded mRNA-Seq Library Preparation Kit	Illumina	Cat# 20020594
ESM1 ELISA KIT	BosterBio	Cat# EK0752
Ponatinib	Selleckchem	Cat# S1490
Deposited Data		
RNA sequencing data	This study	GEO accession# GSE137809
RNA sequencing data expression	This study	Table S1
ATAC-seq data	This study	GEO accession# GSE137809
ATAC sequencing data expression	This study	Table S2, S3
Experimental Models: Cell Lines		
Normal Human Astrocytes	Lonza	Cat# CC-2565
HBEC-5i	ATCC	Cat# CRL-3245
hG157	Mao et al., 2013[47][47][46][45][44][45][44][44][44][44][44][44][43]	See Table S4
hG711	(Bhat et al., 2013)	See Table S4

hG1051	(Minata et al., 2019)	See Table S4
hG1079	(Minata et al., 2019)	See Table S4
TEC15	This study	See Table S4
293FT	Thermofisher	Cat#R70007
mG7080	(Sadahiro et al., 2018)	N/A
PDGFBB1	This study	N/A
Experimental Models: Organisms/Strains		
NOD scid mice -Prkdc^{scid}	The Jackson Laboratory	Cat# 001303
C57BL6	The Jackson Laboratory	Cat# 000664
ESM1 knockout mice	(Rocha et al., 2014)	N/A
Oligonucleotides		
Primers for qRT-PCR	This study	See Methods section
Recombinant DNA		
psPAX2	Addgene	Cat# 12260
GFP	Addgene	N/A
mCherry	Addgene	N/A
pMD2.G	Addgene	Cat# 12259
Software and Algorithms		
GraphPad Prism	GraphPad Software N/A	N/A
FlowJo 10	FLOWJO, LLC	N/A
ImageJ	NIH	N/A
Ingenuity Pathway Analysis	Qiagen	N/A

634 Supplemental Table S5: Oligonucleotides

Species	Sequences
Human 18S	Forward: GGCCCTGTAATTGGAATGAGTC Reverse: CCAAGATCCAACTACGAGCTT
Human ESM1	Forward: TCCCGGCTGTGATTTCTGAG Reverse: ACCATGCATCACATTTGGTCTTC
Human NFκB:	Forward: CCT GGA TGA CTC TTG GGA AA Reverse: TCA GCC AGC TGT TTC ATG TC
Human PDGFRα	Forward: AGGGATAGCTTCCTGAGCCA

	Reverse: AGCTCCGTGTGCTTTCATCA
Human Bactin	Forward: AGAAGAGCTATGAGCTGCCTGACG Reverse: TACTTGCGCTCAGGAGGAGCAATG
Human GAPDH	Forward: GAA GGT GAA GGT CGG AGT CA Reverse: TTG AGG TCA ATG AAG GGG TC
Mouse Podocalyxin	Forward: TACTGTCGCCTGCATCTCAC Reverse: TGATGTTGTGGCACTTTGGT
Mouse SMa	Forward: AGACAGCTATGTGGGGGATG Reverse: CTTTTCCATGTCGTCCCAGT
Mouse Occludin	Forward: GCGGAAAGAGTTGACAGTCC Reverse: GGCACCAGAGGTGTTGACTT
Mouse CD31	Forward: GCCCAATCACGTTTCAGTTT Reverse: AAAACGCTTGGGTGTCATTC
Mouse Claudin5	Forward: AAATTCTGGGTCTGGTGCTG Reverse: GTCACGATGTTGTGGTCCAGM
Mouse PEDF	Forward: ACCGTGACCCAGAACTTGAC Reverse: GACAGTCAGCACAGCTTGGA
Mouse GAPDH	Forward: GTT GTC TCC TGC GAC TTC Reverse: GGT GGT CCA GGG TTT CTT

Mouse VWF	Forward: CAGCATCTCTGTGGTCCTGA Reverse: GGAGGCTGCTAGTGGTGAAG

REFERENCES

1. Kuhnt, D., et al., *Correlation of the extent of tumor volume resection and patient survival in surgery of glioblastoma multiforme with high-field intraoperative MRI guidance.* Neuro-Oncology, 2011. **13**(12): p. 1339-1348.
2. Sottoriva, A., et al., *Intratumor heterogeneity in human glioblastoma reflects cancer evolutionary dynamics.* Proc Natl Acad Sci U S A, 2013. **110**(10): p. 4009-14.
3. Brennan, C.W., et al., *The somatic genomic landscape of glioblastoma.* Cell, 2013. **155**(2): p. 462-77.
4. Li, C., et al., *Tumor Edge-to-Core Transition Promotes Malignancy in Primary-to-Recurrent Glioblastoma Progression in a PLAGL1/CD109-mediated mechanism.* bioRxiv, 2020: p. 2020.09.14.293753.
5. Bastola, S., et al., *Glioma-initiating cells at tumor edge gain signals from tumor core cells to promote their malignancy.* Nat Commun, 2020. **11**(1): p. 4660.
6. Spiteri, I., et al., *Evolutionary dynamics of residual disease in human glioblastoma.* Ann Oncol, 2019. **30**(3): p. 456-463.
7. Minata, M., et al., *Phenotypic Plasticity of Invasive Edge Glioma Stem-like Cells in Response to Ionizing Radiation.* Cell Rep, 2019. **26**(7): p. 1893-1905 e7.
8. Jin, X., et al., *Targeting glioma stem cells through combined BMI1 and EZH2 inhibition.* Nature Medicine, 2017. **23**(11): p. 1352-1361.
9. Lasocki, A. and F. Gaillard, *Non-Contrast-Enhancing Tumor: A New Frontier in Glioblastoma Research.* American Journal of Neuroradiology, 2019.
10. Yan, J.-L., et al., *Multimodal MRI characteristics of the glioblastoma infiltration beyond contrast enhancement.* Therapeutic advances in neurological disorders, 2019. **12**: p. 1756286419844664-1756286419844664.
11. Yamashita, D., et al., *Targeting glioma-initiating cells via the tyrosine metabolic pathway.* J Neurosurg, 2020: p. 1-12.
12. Ibrahim, A.N., et al., *Intratumoral spatial heterogeneity of BTK kinomic activity dictates distinct therapeutic response within a single glioblastoma tumor.* J Neurosurg, 2019: p. 1-12.
13. Pavlyukov, M.S., et al., *Apoptotic Cell-Derived Extracellular Vesicles Promote Malignancy of Glioblastoma Via Intercellular Transfer of Splicing Factors.* Cancer Cell, 2018. **34**(1): p. 119-135 e10.
14. Holash, J., et al., *Vessel cooption, regression, and growth in tumors mediated by angiopoietins and VEGF.* Science, 1999. **284**(5422): p. 1994-8.
15. Hambardzumyan, D. and G. Bergers, *Glioblastoma: Defining Tumor Niches.* Trends Cancer, 2015. **1**(4): p. 252-265.
16. Calabrese, C., et al., *A perivascular niche for brain tumor stem cells.* Cancer Cell, 2007. **11**(1): p. 69-82.
17. Charles, N., et al., *Perivascular nitric oxide activates notch signaling and promotes stem-like character in PDGF-induced glioma cells.* Cell Stem Cell, 2010. **6**(2): p. 141-52.
18. Christensen, K., H.D. Schroder, and B.W. Kristensen, *CD133+ niches and single cells in glioblastoma have different phenotypes.* J Neurooncol, 2011. **104**(1): p. 129-43.
19. Christensen, K., H.D. Schroder, and B.W. Kristensen, *CD133 identifies perivascular niches in grade II-IV astrocytomas.* J Neurooncol, 2008. **90**(2): p. 157-70.
20. Burgett, M.E., et al., *Direct contact with perivascular tumor cells enhances integrin alphavbeta3 signaling and migration of endothelial cells.* Oncotarget, 2016. **7**(28): p. 43852-43867.
21. Lassalle, P., et al., *ESM-1 is a novel human endothelial cell-specific molecule expressed in lung and regulated by cytokines.* J Biol Chem, 1996. **271**(34): p. 20458-64.
22. Kali, A. and K.S. Shetty, *Endocan: a novel circulating proteoglycan.* Indian J Pharmacol, 2014. **46**(6): p. 579-83.
23. Scherpereel, A., et al., *Overexpression of endocan induces tumor formation.* Cancer Res, 2003. **63**(18): p. 6084-9.
24. Maurage, C.A., et al., *Endocan expression and localization in human glioblastomas.* J Neuropathol Exp Neurol, 2009. **68**(6): p. 633-41.
25. Almog, N., et al., *Transcriptional switch of dormant tumors to fast-growing angiogenic phenotype.* Cancer Res, 2009. **69**(3): p. 836-44.

26. Rocha, S.F., et al., *Esm1 modulates endothelial tip cell behavior and vascular permeability by enhancing VEGF bioavailability.* Circ Res, 2014. **115**(6): p. 581-90.
27. Herting, C.J., et al., *Tumour-associated macrophage-derived interleukin-1 mediates glioblastoma-associated cerebral oedema.* Brain, 2019. **142**(12): p. 3834-3851.
28. Zhu, Y., et al., *Early inactivation of p53 tumor suppressor gene cooperating with NF1 loss induces malignant astrocytoma.* Cancer Cell, 2005. **8**(2): p. 119-30.
29. Hemmati, H.D., et al., *Cancerous stem cells can arise from pediatric brain tumors.* Proceedings of the National Academy of Sciences, 2003. **100**(25): p. 15178-15183.
30. Laks, D.R., et al., *Neurosphere formation is an independent predictor of clinical outcome in malignant glioma.* Stem Cells, 2009. **27**(4): p. 980-7.
31. Heldin, C.H. and B. Westermark, *Mechanism of action and in vivo role of platelet-derived growth factor.* Physiological Reviews, 1999. **79**(4): p. 1283-1316.
32. Heldin, C.H., A. Ostman, and L. Rönnstrand, *Signal transduction via platelet-derived growth factor receptors.* Biochim Biophys Acta, 1998. **1378**(1): p. F79-113.
33. Hermanson, M., et al., *Platelet-derived growth factor and its receptors in human glioma tissue: expression of messenger RNA and protein suggests the presence of autocrine and paracrine loops.* Cancer Res, 1992. **52**(11): p. 3213-9.
34. Betsholtz, C., *Biology of platelet-derived growth factors in development.* Birth Defects Res C Embryo Today, 2003. **69**(4): p. 272-85.
35. Ozawa, T., et al., *PDGFRA gene rearrangements are frequent genetic events in PDGFRA-amplified glioblastomas.* Genes Dev, 2010. **24**(19): p. 2205-18.
36. Martinho, O., et al., *Expression, mutation and copy number analysis of platelet-derived growth factor receptor A (PDGFRA) and its ligand PDGFA in gliomas.* Br J Cancer, 2009. **101**(6): p. 973-82.
37. Jackson, E.L., et al., *PDGFR alpha-positive B cells are neural stem cells in the adult SVZ that form glioma-like growths in response to increased PDGF signaling.* Neuron, 2006. **51**(2): p. 187-99.
38. Roskoski, R., Jr., *The role of small molecule platelet-derived growth factor receptor (PDGFR) inhibitors in the treatment of neoplastic disorders.* Pharmacol Res, 2018. **129**: p. 65-83.
39. Buenrostro, J.D., et al., *ATAC-seq: A Method for Assaying Chromatin Accessibility Genome-Wide.* Curr Protoc Mol Biol, 2015. **109**: p. 21 29 1-9.
40. Cavallin, L.E., et al., *KSHV-induced ligand mediated activation of PDGF receptor-alpha drives Kaposi's sarcomagenesis.* PLOS Pathogens, 2018. **14**(7): p. e1007175.
41. Tamura, R., et al., *Visualization of spatiotemporal dynamics of human glioma stem cell invasion.* Molecular Brain, 2019. **12**(1): p. 45.
42. de Groot, J.F., et al., *Tumor invasion after treatment of glioblastoma with bevacizumab: radiographic and pathologic correlation in humans and mice.* Neuro Oncol, 2010. **12**(3): p. 233-42.
43. Neftel, C., et al., *An Integrative Model of Cellular States, Plasticity, and Genetics for Glioblastoma.* Cell, 2019. **178**(4): p. 835-849.e21.
44. Alcantara Llaguno, S., et al., *Malignant Astrocytomas Originate from Neural Stem/Progenitor Cells in a Somatic Tumor Suppressor Mouse Model.* Cancer Cell, 2009. **15**(1): p. 45-56.
45. Gotlib, L.J. and D.B. Searls, *Plasma membrane isolation on DEAE-Sephadex beads.* Biochim Biophys Acta, 1980. **602**(1): p. 207-12.
46. Xiao, W., et al., *Hyaluronic-Acid Based Hydrogels for 3-Dimensional Culture of Patient-Derived Glioblastoma Cells.* J Vis Exp, 2018(138).
47. Mao, P., et al., *Mesenchymal glioma stem cells are maintained by activated glycolytic metabolism involving aldehyde dehydrogenase 1A3.* Proceedings of the National Academy of Sciences of the United States of America, 2013. **110**(21): p. 8644-8649.

Figure Legends

Figure 1. Tumor-associated VE cells promote glioblastoma aggressiveness in vivo, accompanied by their secretion of endocan

(A) Pre-operation MRI T1-weighted, and perfusion Magnetic Resonance imaging (MRI) of a glioblastoma patient highlighting necrotic core (enhancing on T1, blue intensity on perfusion) and vasculature-rich edge (enhancing on T2, green intensity on perfusion) areas.

(B) Kaplan-Meier survival analysis of SCID mice following intracranial injection of glioma spheres (hG1051) or glioma spheres (hG1051) +Tumor Endothelial cells (TEC15) at 1:10 ratio. ***P=0.003, log-rank test (n=5 mice per group).

(C) Schematic outlining the screening procedure to identify paracrine signals of VE cells from 8 glioblastoma patient samples.

(D) Volcano plot of RNA-sequencing (RNA-seq) data comparing gene expressions of normal and tumor endothelial cells, with Es(red arrow). FC=9.76, FDR-corrected p-value=0.0031.

(E)TCGA LGG and HGG cohort to compare expression of endocan in TCGA's WHO grade II, III, and IV tumors.

(F) Depiction of SMC cohort data set showing the level of endocan expression in grade IV Glioma.

(G) Kaplan-Meier analysis showing the correlation between endocan expression and the survival of 667 glioma patients. P = 0.044, by log-rank test.

(H) ELISA comparing levels of secreted endocan in CM from NHA, HBEC-5i, g157, g711 and g1051. *P=0.0001; two-tailed Student's t-test. Scale bar, 50 μm. All quantitative data are average ±SD; *P<0.01, **P<0.001, ***P<0.0001.

(I) Representative immunofluorescence (IF) staining of endocan or CD31 in formalin-fixed paraffin-embedded tissue sections from glioblastoma patient hG1051. Nuclei stained with DAPI. Scale bar, 50 μm. All quantitative data are average ±SD; **P*<0.01, ***P*<0.001, ****P*<0.0001.

Figure 2. Endocan is required for establishing the hypervascular tumor edge structure in murine glioblastoma

(A) Murine glioblastoma tissues collected from tumor formed in Nestin-Tva/Cdkn2a-/- mice formed by RCAS-PDGFB injection. Tumor was obtained, sliced into single cells and injected into WT or *Esm1* KO mice, gross images from WT and KO mice brains (upper). H&E (middle).

(B) CD31 staining (lower) of WTD or *Esm1* KOD tumor and non-tumor bearing brain hemispheres. Scale bar, 200 μm.

(C) mg7080 murine glioblastoma cells formed in *PTEN/P53/NF1* deleted glioblastoma model. Tumor was obtained and cells were put in culture in neurosphere medium. Gross images depicting brains collected form mG7080 glioma-bearing *Esm1* KO or WT mice (upper). H&E (middle).

(D) CD31 staining (lower) of mG7080 *Esm1* KOD or WTD tumor and non-tumor bearing brain hemispheres. Scale bar, 200 μm.

(E) Transmission electron microscopy (TEM) of WTD and *Esm1* KOD normal and tumor tissues. The following structures are indicated in imaging: Endothelial cell (EC). Scale bar, 500 nm.

Figure 3. Endocan-driven edge+core and endocan-depleted core lesions cooperatively increase intratumoral heterogeneity, elevating the malignancy of murine glioblastoma

(A) Schematic outlining injection of mg7080 spheres in WT and *Esm1* KO host, followed by isolation of tumor cells, labeling *Esm1* KO derived spheres with mCherry and WT derived spheres with GFP and co-injection into WT host.

(B) IHC staining for GFP and mCherry positive cells in co-injected WT host brain indicating the migration pattern of tumor cells. Injection site indicated by *.

(C) IHC staining for the VE marker (CD31), and hypovascularity markers (HIF1α, ALDH1A3, and YKL-40) in co-injected *Esm1* WT-GFP + KO-mCherry mice brain tumors comparing core (upper) and edge (lower) areas (n=5 mice per group).

(D) DAB intensity analysis scoring for respective tumor edge and core areas (lower). Scale bar, 200 μm. *t*-test, $^{**}P<0.01$, $^{***}P<0.001$; n=6; s.d. (error bar).

(E) IHC staining for GFP and mCherry positive cells in co-injected *Esm1* KO host brain indicating the migration pattern of tumor cells. Injection site indicated by *.

(F, G) Kaplan-Meier survival analysis for WT or *Esm1* -/-mice following intracranial injection of *Esm1* KO-mCherry, WT-GFP or both (mix) at 1:1 ratio. (n=5 mice per group), $^{*}P=0.047$; by comparing 1:1 mix and WT. ns $P=0.31$; by comparing WT and *Esm1* KO. $^{**}P=0.00642$; by comparing 1:1 mix and *Esm1* KO. *P*-values were determined by log-rank test. All quantitative data are average ±SD; $^{*}P<0.01$, $^{**}P<0.001$, $^{***}P<0.0001$, two-tailed Student's *t*-test.

Figure 4. Endocan binds to and phosphorylates PDGFRα in human glioblastoma cells

(A) Schematic outlining identification of PDGFRα as a receptor of Endocan via rhEndocan knockdown of hG157 cells followed by mass spectrometry.

(B) Immunoprecipitation (IP) Western blot (WB) demonstrating binding of exogenous His-tagged rhEndocan and Fc-tagged rhPDGFRα.

(C) Graphical comparison of endocan binding intensities following administration of 0-10 ug/ml PDGFBB or endocan to hG1079 cells

(D) Adjacent slide IHCs for endocan (left) and PDGFRα (right) of glioblastoma patient 101027 tumor samples.

(E) WB comparing phosphorylation of PDGFRα (Y720) following the addition of 10ng/ml rhEndocan or rhPDGFBB, measured at distinct time-points. WB comparing phosphorylation of downstream targets of PDGFRα (Y720) following the addition of 10ng/ml rhEndocan or rhPDGFBB, measured at distinct time-points.

(F) WB comparing phosphorylation of downstream PDGFRα targets following the addition of 10ng/ml of rhEndocan or rhPDGFBB, measured at distinct time-points.

(G) Kaplan Meier survival analysis of Bl/6 mice following intracranial injection of WT-GFP and KO-mCherry cells. Mice were treated with 50mg/kg/day dose of ponatinib for 5 days, compared to control. **P*<0.046. *P*-value was determined by log-rank test.

(H) IHC staining of tumor-bearing mice brains following intracranial for mCherry, PDGFRα, Olig2, pP65-NF-κB in control (upper), Ponatinib treated group (lower). Mice were treated with 50mg/kg/day compared to control. DAB intensity analysis scoring for respective tumors (lower). *t*-test, ****P*<0.001; n=5; s.d. (error bar). All quantitative data are average ±SD; **P*<0.01, ***P*<0.001, ****P*<0.0001, two-tailed Student's *t*-test.

Figure 5. Endocan-mediated signaling alters chromatin accessibility in glioblastoma cells, including the promoter region of the Myc gene

(A) ATAC-seq analysis for WTD and *Esm1* KOD tumors shows changes in WTD vs. KOD tumors (n=2 mice per group).

(B) ATAC-seq and RNA-seq analysis for the Myc gene from WTD and *Esm1* KOD tumors.

(C) MYC gene is implicated in *Esm1* KOD tumors (shown by red arrow) in RNA-seq data.

(D) IHC analysis for WTD and *Esm1* KOD tumors for MYC expression.

(E) Schema highlighting the edge like phenotype conferred by endocan.

Figure 6. Endocan protects edge-located glioblastoma cells from radiotherapy-induced cell death *in vivo*

(A) ELISA for secreted endocan from HBEC-5i cells in CM following irradiation with 8 Gy at 1, 2, 3 time-points. ****P<0.0001, 2-tailed t-test.

(B) *In vitro* radio-sensitivity assay for glioma spheres (g157, g711, g267, g1079) pretreated with rhEndocan for 3 days and irradiated on Day 3. Cell growth was measured on Day 7. **P<0.01, ***P<0.001, 2-tailed t-test.

(C) Alamar Blue to measure the cell growth post radiation for Control, IgG and endocan blocking in HBEC-5i CM. ***P<0.001, ****P<0.0001, 2-tailed t-test. (D) H&E of *Esm1* WTD (upper) or KOD (lower) mice brains following intracranial injection of mG7080 cells and administration of 2.5 Gy irradiation for 3 days. Mice were sacrificed 2 weeks post-radiotherapy. Mice brain slices were compared to sham-irradiated mice. n=5 mice.

(E)Kaplan Meier survival analysis of *Esm1* WT or *Esm1* -/- mice following intracranial injection of mG7080 cells. Mice were radiated with 2.5 Gy for 3 days and were monitored for tumor burden. P-value was determined by log-rank test.

(F) Gene-set enrichment analysis using Gene Ontology database comparing genes upregulated and downregulated after treatment with endocan and VE CM (2-fold or higher). All quantitative data are average ±SD; *P<0.01, **P<0.001, ***P<0.0001.

Supplementary Figure Legends

Supplementary Figure 1: related to Figure 1

(A)Pre-operation and post-operation MRI T1-weighted, and perfusion Magnetic Resonance imaging (MRI) of a glioblastoma patient highlighting necrotic core (enhancing on T1, blue intensity on perfusion) and vasculature-rich edge (enhancing on T2, green intensity on perfusion) areas.

Supplementary Figure 2: related to Figure 1

(A) MRI T1-weighted, and perfusion Magnetic Resonance imaging (MRI) of a glioblastoma patient highlighting necrotic core (enhancing on T1, blue intensity on perfusion) and vasculature-rich edge (enhancing on T2, green intensity on perfusion) areas. Microscopic intra-operative view highlights edge and core areas (edge indicated by white line and arrows, core indicated by yellow line and arrow).

(B)Schema showing isolation of patient derived vascular endothelial cells.

(C) Kaplan-Meier survival analysis of SCID mice following intracranial injection of g1051 or g1051+HBEC-5i cells at 1:10 ratio. ***P=0.003, log-rank test (n=5 mice per group) ***P <0.001, by log-rank test.(D) Representative immunohistochemistry (IHC) staining of CD31(red) in mice glioblastoma tumors formed in control (upper) or hG1051+TEC15 co-injection (lower) groups. (n=5 mice per group). Scale bar, 100 μm.

Supplementary Figure 3: related to Figure 2

(A)Normal H&E and CD31 staining in non-tumor section in these two tumor models.

(B) Representative images of g1005 and g1037 spheres with and without endocan under the *in vitro* migration-inducing condition when they were encapsulated in hydrogels.

Supplementary Figure 4: related to Figure 4

(A) Box plot showing PLA signals of PDGFRα or rhEndocan, rhPDGFBB, and control group. hG1051 cells were used. 2-tailed *t*-test, *P<0.05, ***P<0.001. s.d. (error bar).

(B) Graphical comparison of endocan and PDGFBB binding intensities following administration of 0-10 ug/ml PDGFBB or endocan to hG1079 cells.

(C) GSEA for comparisons of RNA-seq data from tumors in WTD and KOD mice (A) to gene sets representing angiogenesis genes.

(D) qRT-PCR for vascular associated genes in tumors from WTD and KOD mice. All quantitative data are average ±SD; **P*<0.01, ***P*<0.001, ****P*<0.0001, two-tailed Student's *t*-test.

Supplementary Figure 5: related to Figure 5

(A) qRT-PCR for *ESM1* from HBEC-5i cells treated with 50μM TMZ treatment 24 and 48 hrs after treatment.

(B) qRT-PCR measurement of *ESM1* transcripts from HBEC-5i cells following 8Gy irradiation at 24 and 48 hr. *****P*<0.0001, 2-tailed *t*-test.

(C, D) Flow cytometry analysis of caspase 3/7 activity and SYTOX staining of hG1079 cells pretreated with rhEndocan and HBEC-5i CM for 3 days, irradiating it on Day 3 and staining on Day 7. All quantitative data are average ±SD; **P*<0.01, ***P*<0.001, ****P*<0.0001, two-tailed Student's *t*-test.

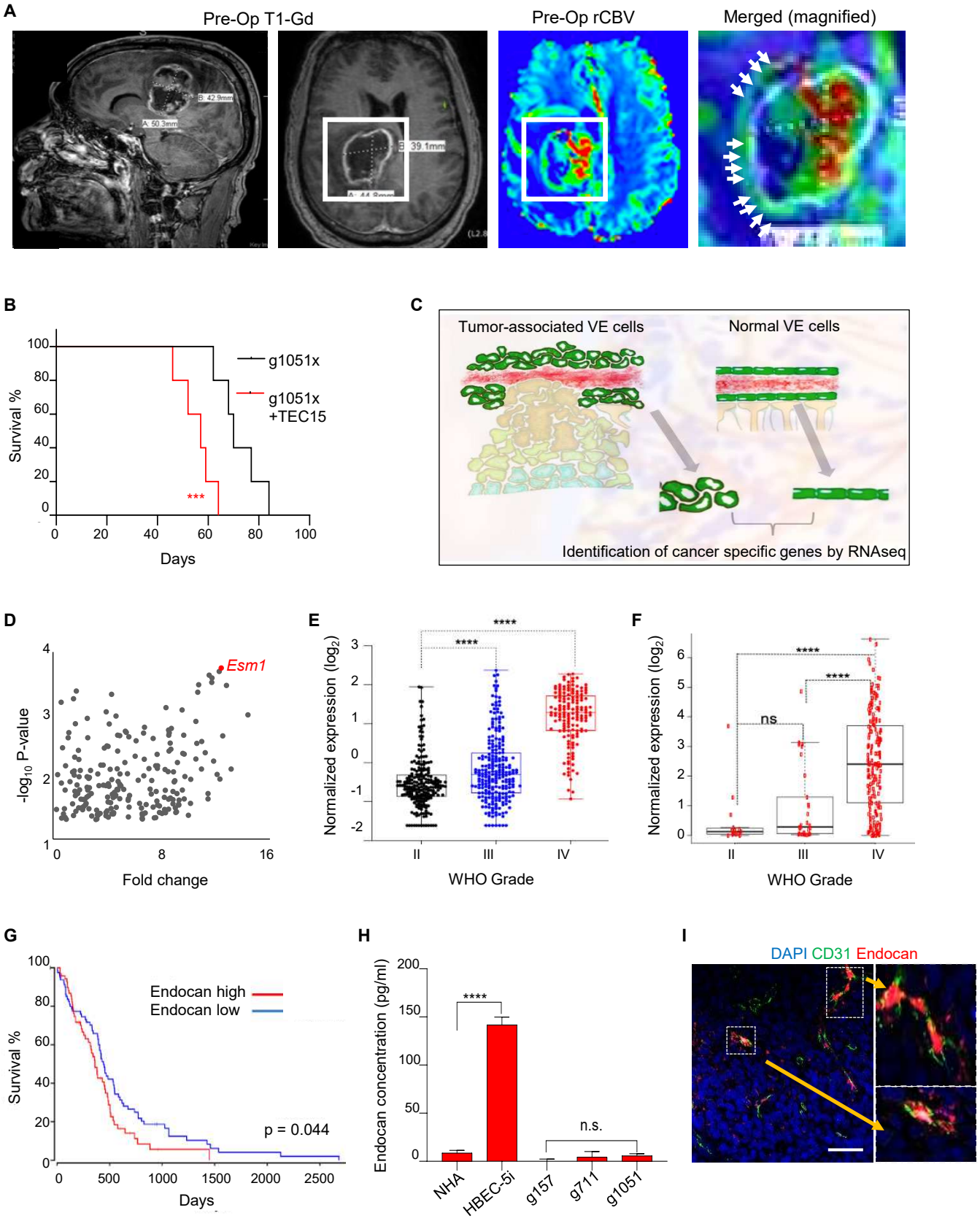
A
Pre-Op T1-Gd
Pre-Op rCBV
Merged (magnified)
B
Survival %
g1051x
g1051x +TEC15
***
Days
C
Tumor-associated VE cells
Normal VE cells
Identification of cancer specific genes by RNAseq
D
Esm1
-log10 P-value
Fold change
E
Normalized expression (log2)
****
WHO Grade
F
Normalized expression (log2)
ns
WHO Grade
G
Survival %
Endocan high
Endocan low
p = 0.044
Days
H
Endocan concentration (pg/ml)
n.s.
NHA
HBEC-5i
g157
g711
g1051
I
DAPI CD31 Endocan

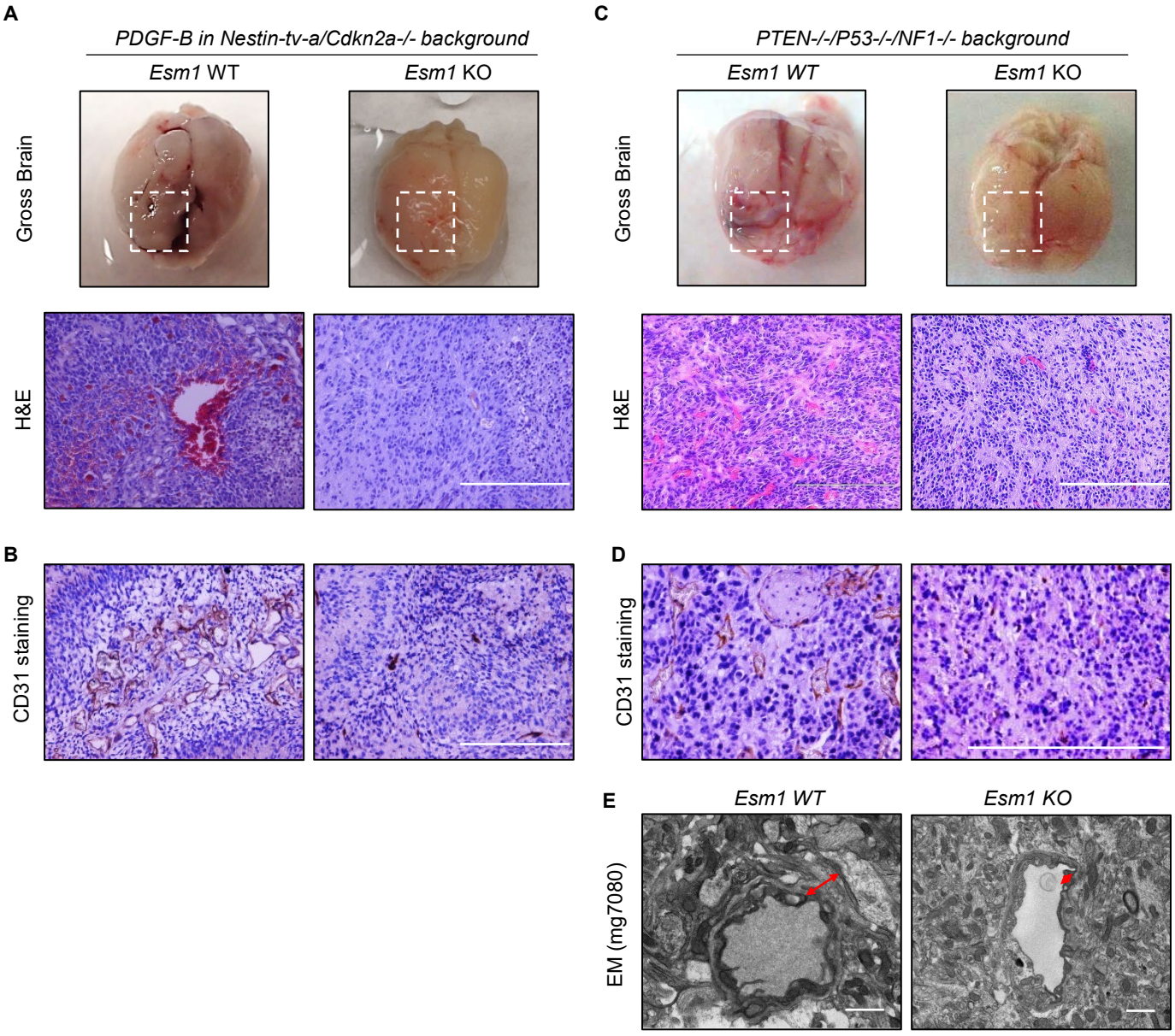
A
PDGF-B in Nestin-tv-a/Cdkn2a-/- background
Esm1 WT
Esm1 KO
Gross Brain
H&E
B
CD31 staining
C
PTEN-/-/P53-/-/NF1-/- background
Esm1 WT
Esm1 KO
Gross Brain
H&E
D
CD31 staining
E
Esm1 WT
Esm1 KO
EM (mg7080)

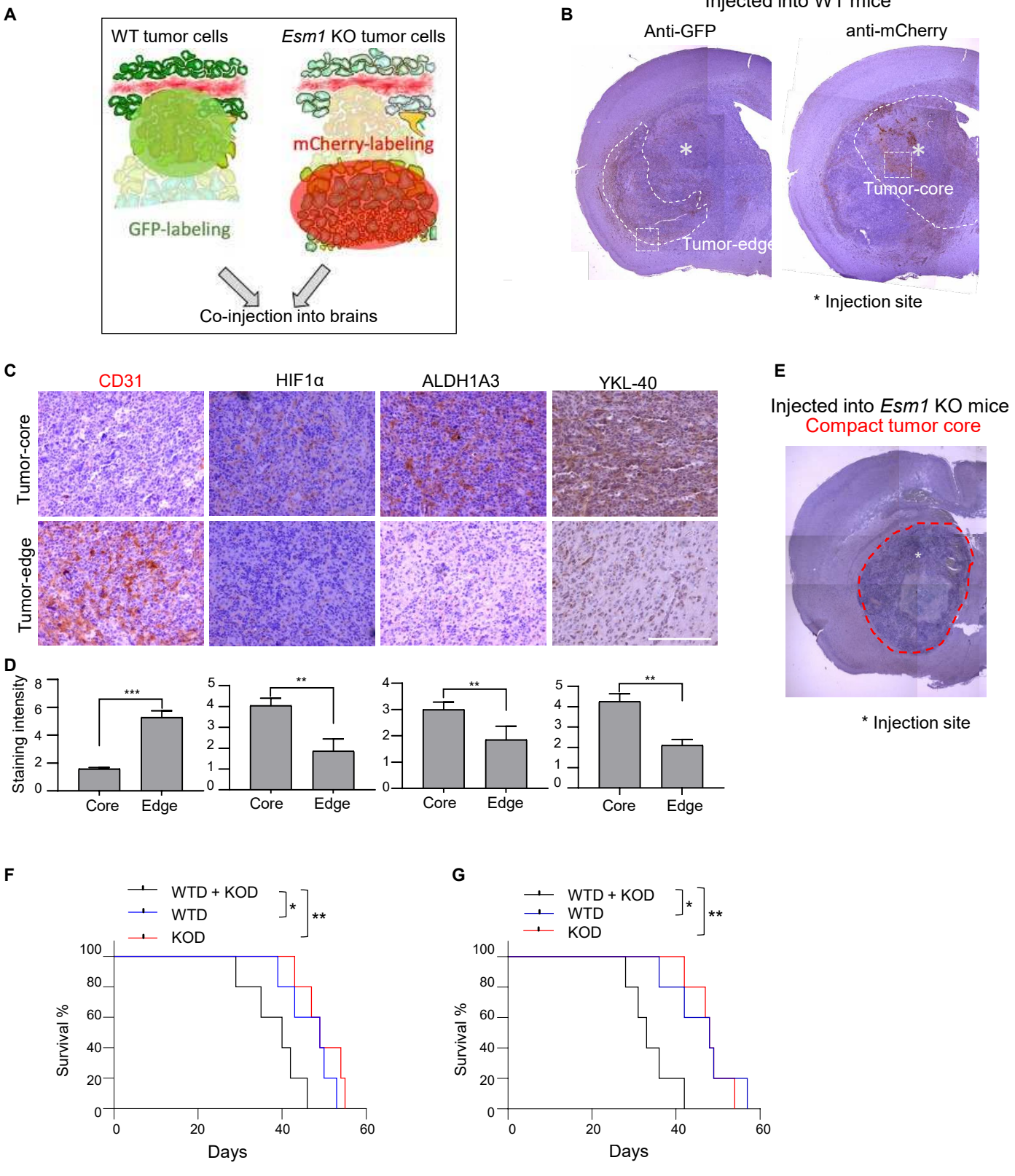
A
WT tumor cells
Esm1 KO tumor cells
mCherry-labeling
GFP-labeling
Co-injection into brains
B
Injected into WT mice
Anti-GFP
anti-mCherry
Tumor-core
Tumor-edge
* Injection site
C
CD31
HIF1α
ALDH1A3
YKL-40
Tumor-core
Tumor-edge
D
Staining intensity
Core
Edge
E
Injected into Esm1 KO mice
Compact tumor core
* Injection site
F
WTD + KOD
WTD
KOD
Survival %
Days
G
WTD + KOD
WTD
KOD
Survival %
Days

Figure 4

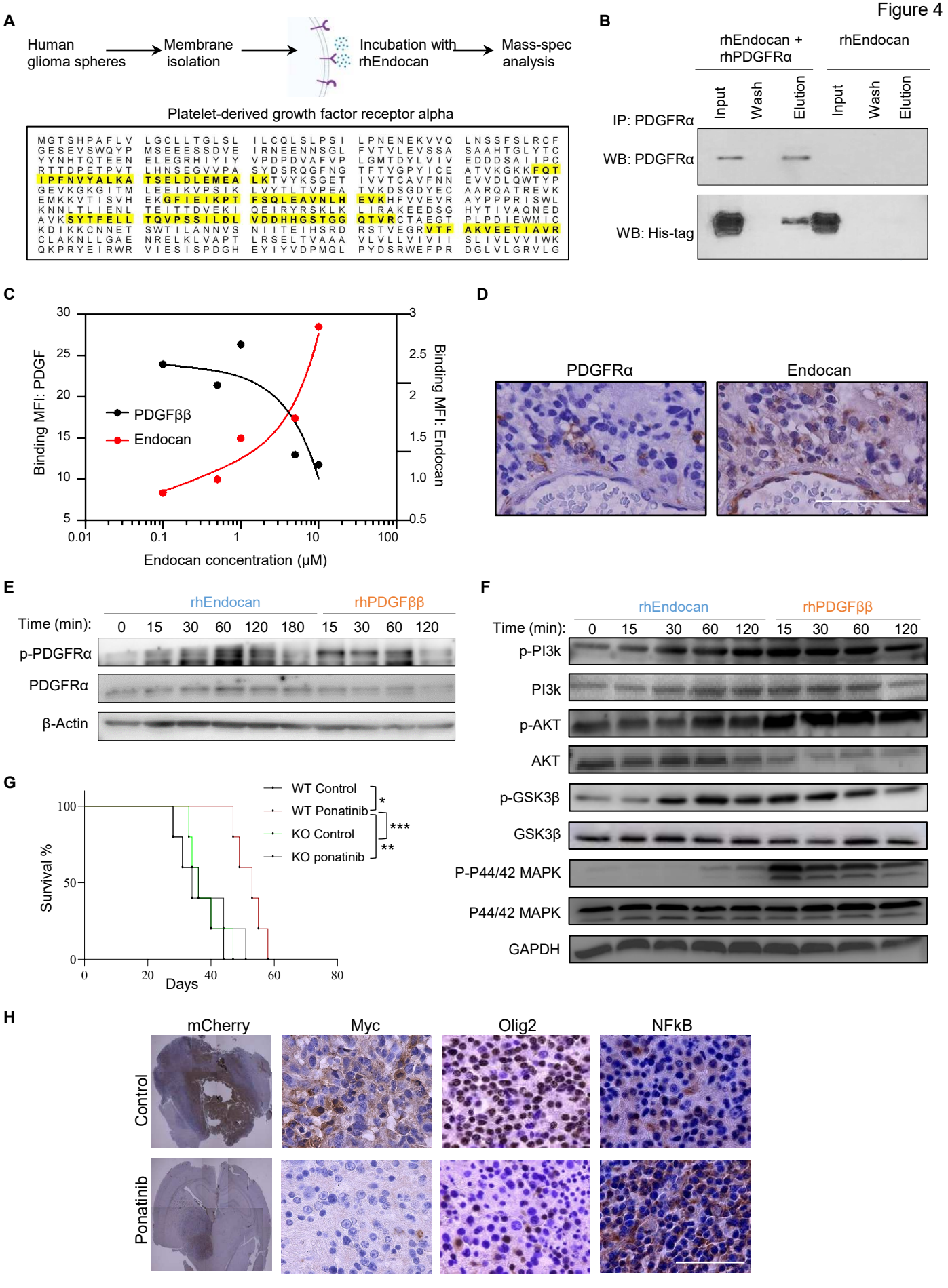
A
Human glioma spheres
Membrane isolation
Incubation with rhEndocan
Mass-spec analysis
Platelet-derived growth factor receptor alpha
B
rhEndocan + rhPDGFRα
rhEndocan
Input
Wash
Elution
IP: PDGFRα
WB: PDGFRα
WB: His-tag
C
Binding MFI: PDGF
Binding MFI: Endocan
PDGFββ
Endocan
Endocan concentration (μM)
D
PDGFRα
Endocan
E
rhEndocan
rhPDGFββ
Time (min):
p-PDGFRα
PDGFRα
β-Actin
F
p-PI3k
PI3k
p-AKT
AKT
p-GSK3β
GSK3β
P-P44/42 MAPK
P44/42 MAPK
GAPDH
G
WT Control
WT Ponatinib
KO Control
KO ponatinib
Survival %
Days
H
mCherry
Myc
Olig2
NFkB
Control
Ponatinib

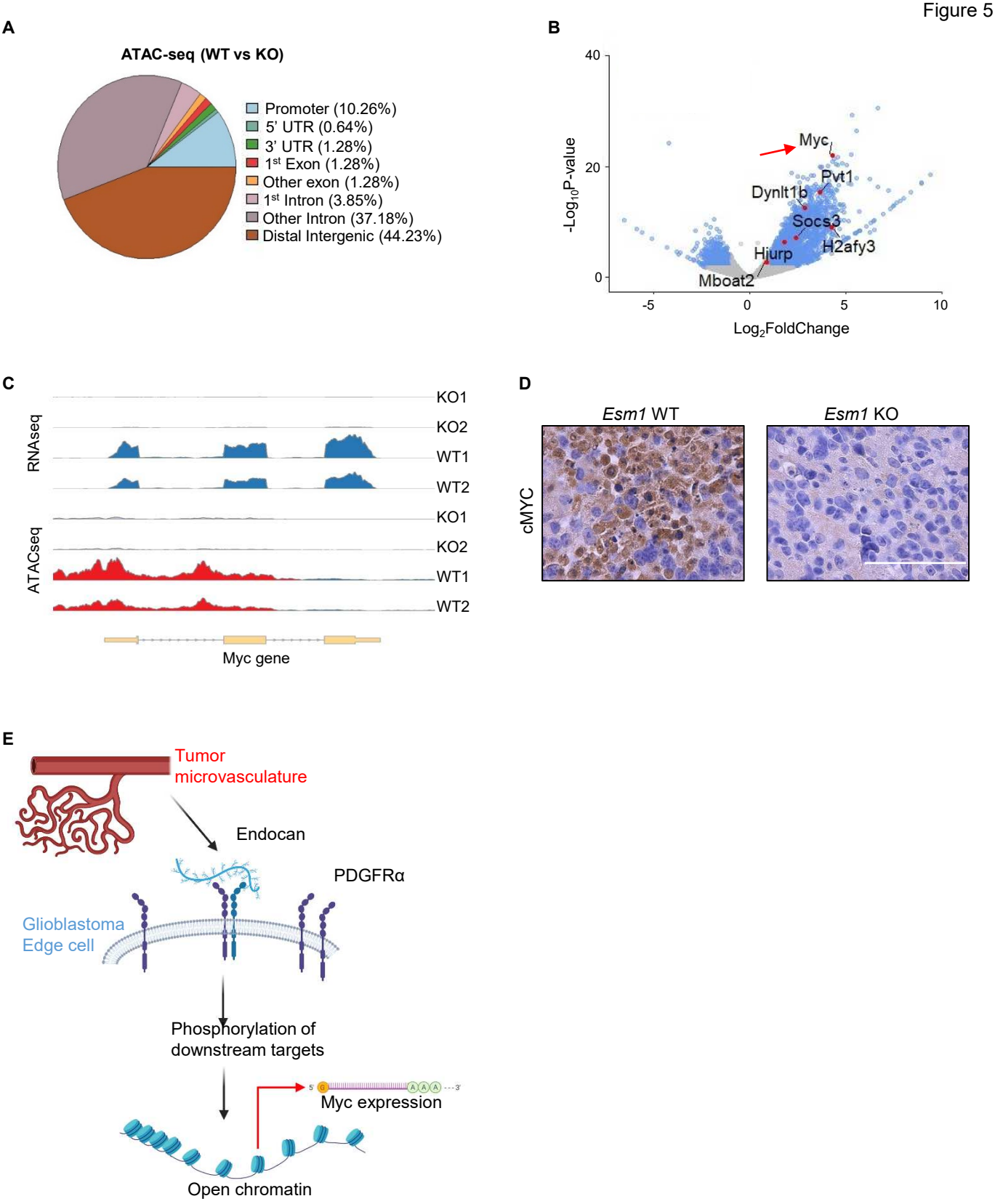
A
ATAC-seq (WT vs KO)
Promoter (10.26%)
5' UTR (0.64%)
3' UTR (1.28%)
1st Exon (1.28%)
Other exon (1.28%)
1st Intron (3.85%)
Other Intron (37.18%)
Distal Intergenic (44.23%)
B
-Log10P-value
Log2FoldChange
Myc
Pvt1
Dynlt1b
Socs3
H2afy3
Hjurp
Mboat2
C
RNAseq
ATACseq
KO1
KO2
WT1
WT2
Myc gene
D
Esm1 WT
Esm1 KO
cMYC
E
Tumor microvasculature
Endocan
PDGFRα
Glioblastoma Edge cell
Phosphorylation of downstream targets
Myc expression
Open chromatin

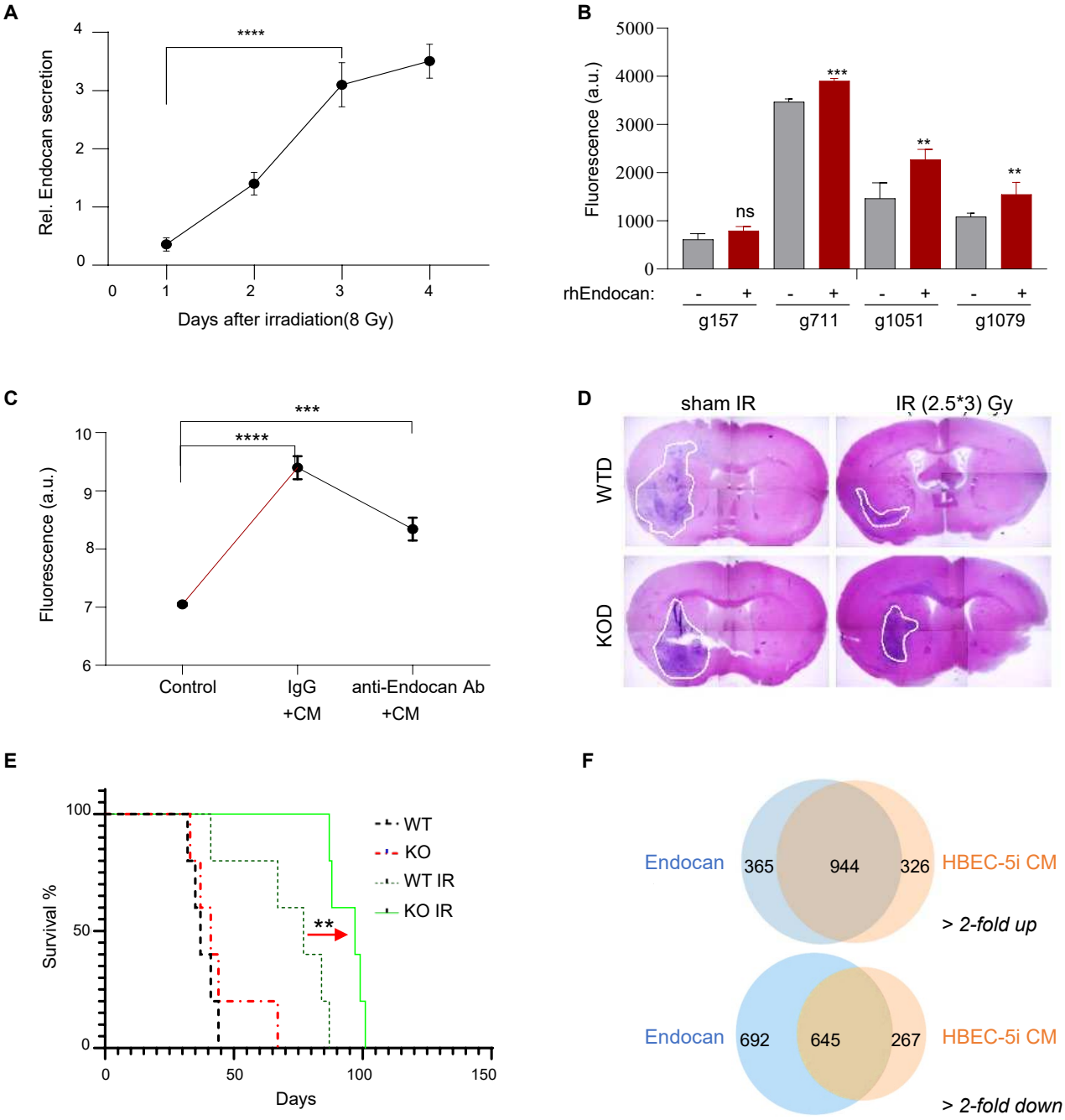
A
Rel. Endocan secretion
Days after irradiation(8 Gy)
****
B
Fluorescence (a.u.)
rhEndocan:
g157
g711
g1051
g1079
ns
***
**
**
C
Fluorescence (a.u.)
Control
IgG +CM
anti-Endocan Ab +CM
***
****
D
sham IR
IR (2.5*3) Gy
WTD
KOD
E
Survival %
Days
WT
KO
WT IR
KO IR
**
F
Endocan
365
944
326
HBEC-5i CM
> 2-fold up
Endocan
692
645
267
HBEC-5i CM
> 2-fold down

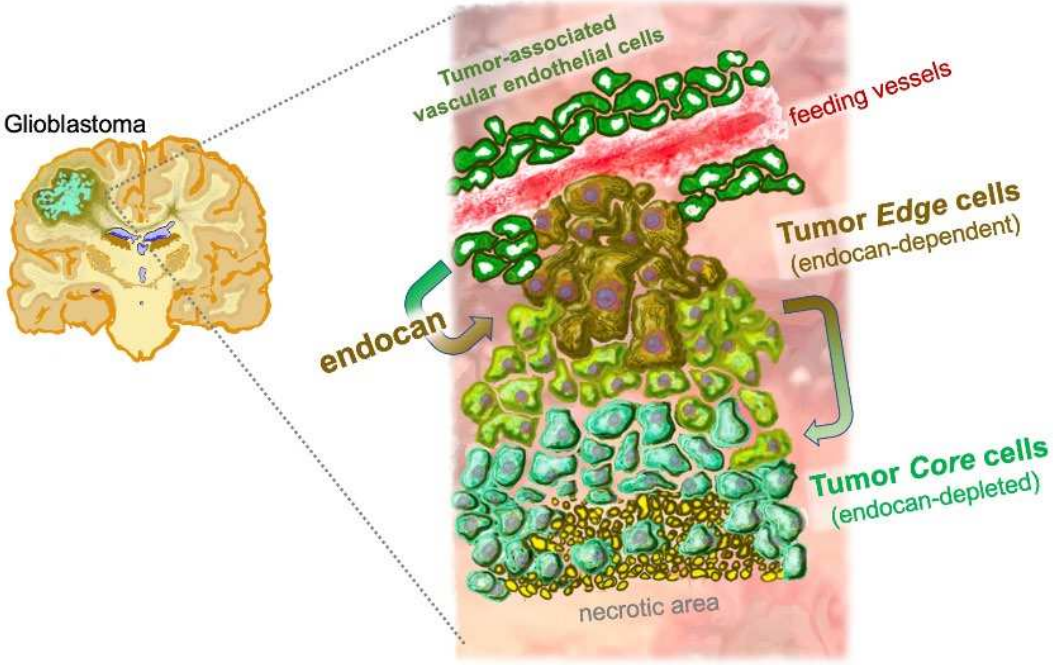
Glioblastoma
Tumor-associated
vascular endothelial cells
feeding vessels
Tumor Edge cells
(endocan-dependent)
endocan
Tumor Core cells
(endocan-depleted)
necrotic area

A

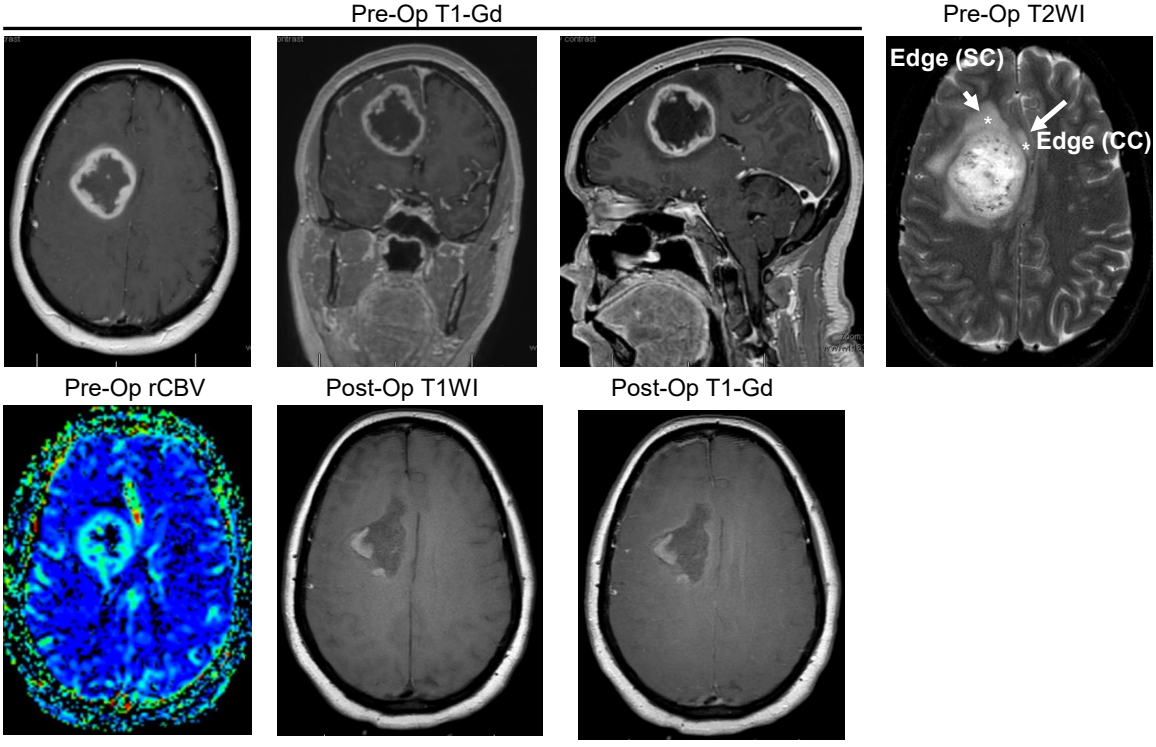
Pre-Op T1-Gd
Pre-Op T2WI
Edge (SC)
Edge (CC)
Pre-Op rCBV
Post-Op T1WI
Post-Op T1-Gd

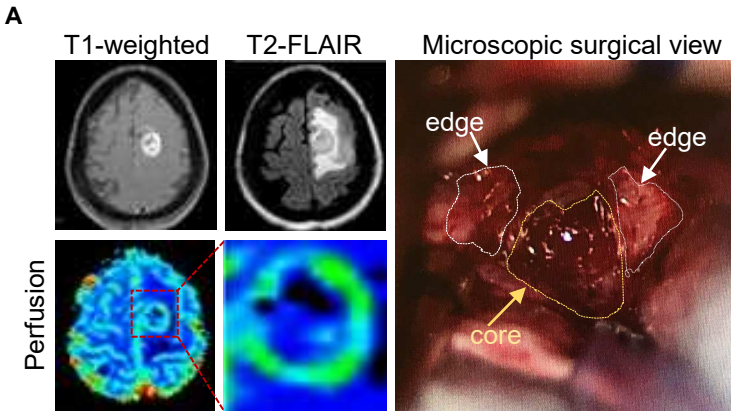
A
T1-weighted
T2-FLAIR
Microscopic surgical view
Perfusion
edge
edge
core

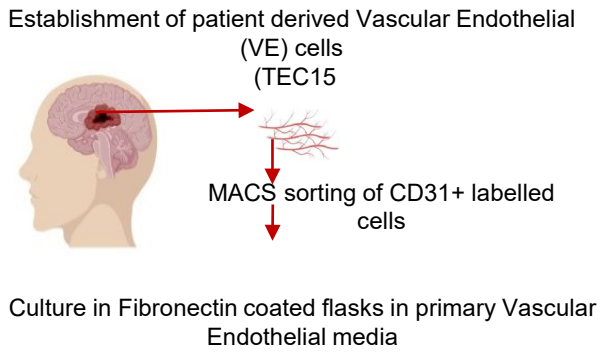
B
Establishment of patient derived Vascular Endothelial (VE) cells (TEC15
MACS sorting of CD31+ labelled cells
Culture in Fibronectin coated flasks in primary Vascular Endothelial media

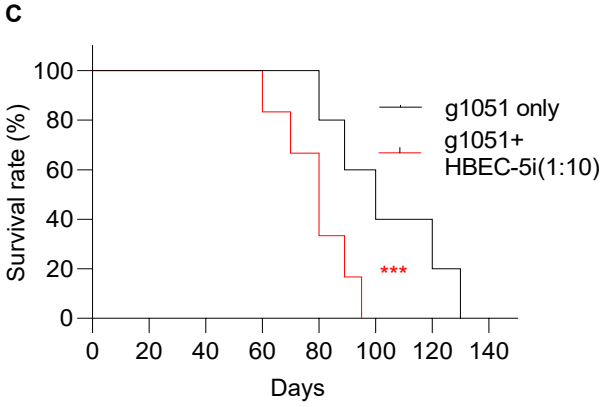
C
Survival rate (%)
100
80
60
40
20
0
0
20
40
60
80
100
120
140
Days
g1051 only
g1051+ HBEC-5i(1:10)
***

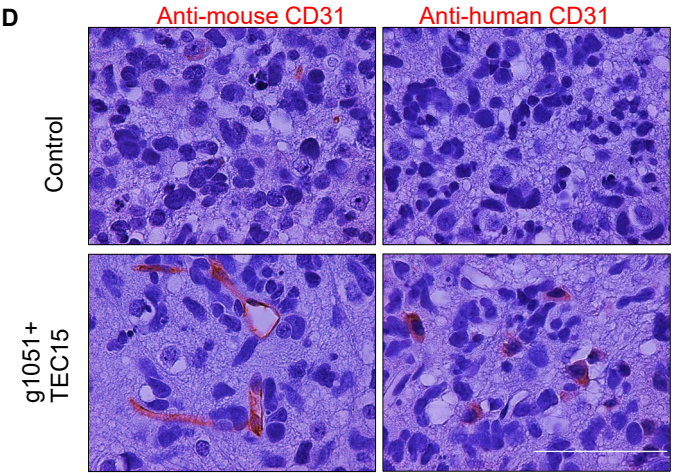
D
Anti-mouse CD31
Anti-human CD31
Control
g1051+ TEC15

A

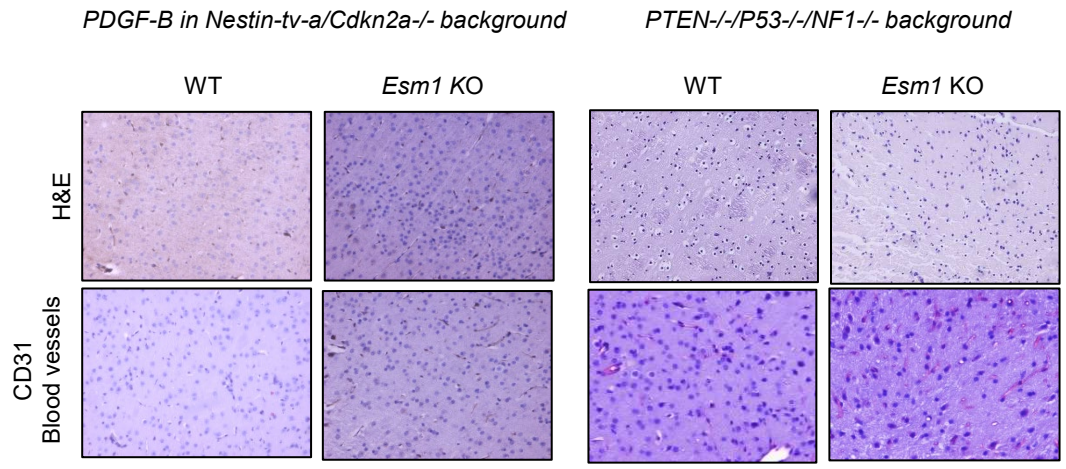
PDGF-B in Nestin-tv-a/Cdkn2a-/- background
PTEN-/-/P53-/-/NF1-/- background
WT
Esm1 KO
WT
Esm1 KO
H&E
CD31
Blood vessels

B

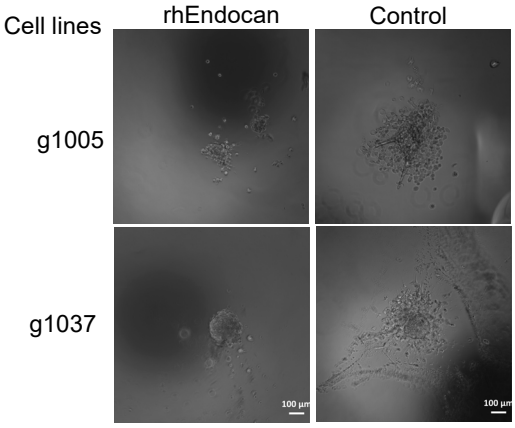
Cell lines
rhEndocan
Control
g1005
g1037
100 µm
100 µm

A

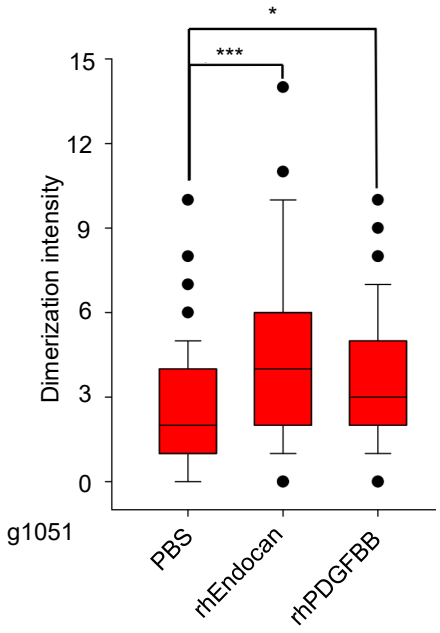

B

	X vs. PDGF	X vs. Endocan
Pearson r		
r	-0.9925	0.9957
95% confidence interval	-0.9933 to -0.9915	0.9952 to 0.9962
R squared	0.9850	0.9915
P value		
P (one-tailed)	<0.001	<0.001
P value summary	***	***
Significant? (alpha = 0.05)	Yes	Yes

C

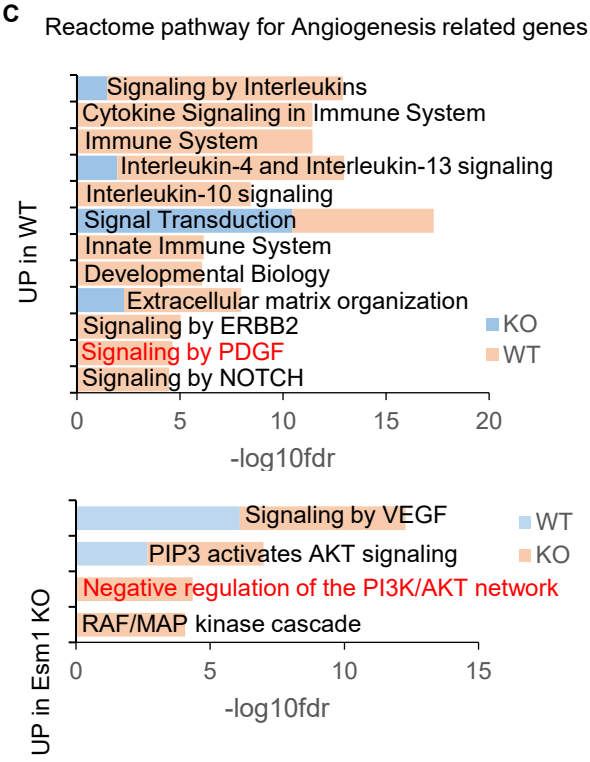

D

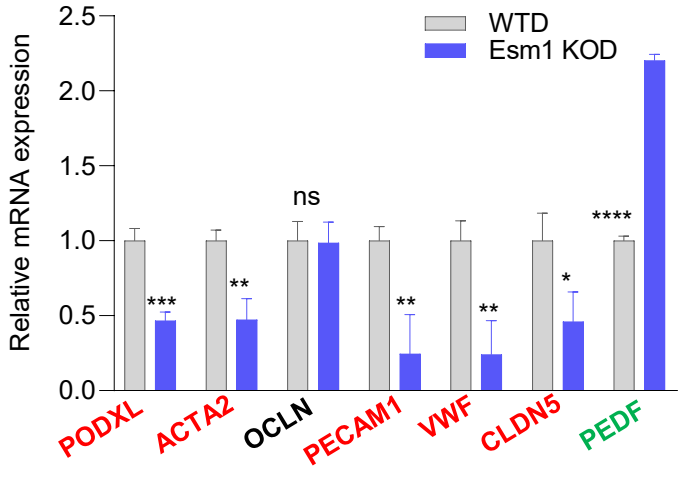

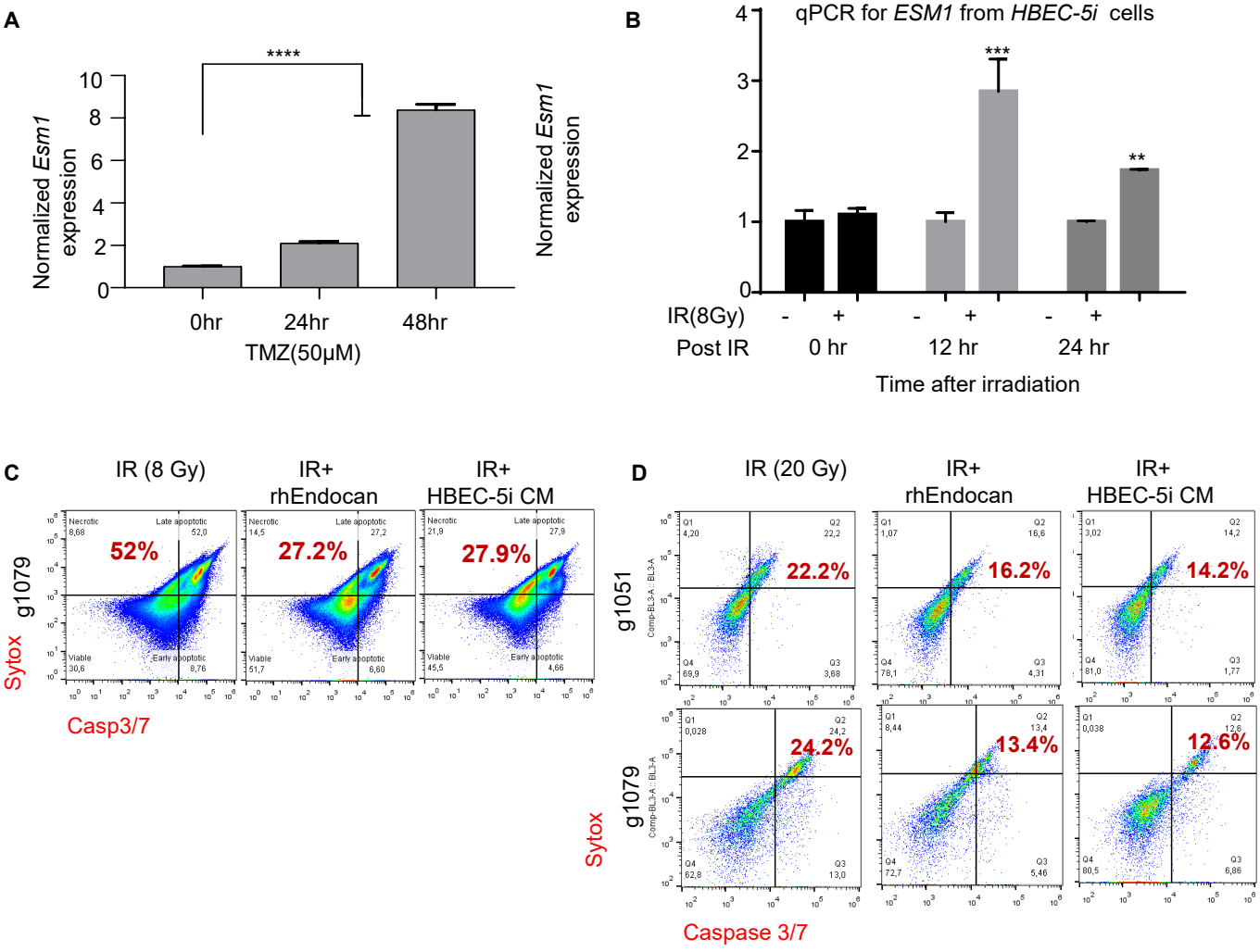
A
****
Normalized Esm1 expression
10
8
6
4
2
0
0hr
24hr
48hr
TMZ(50μM)
Normalized Esm1 expression
B
qPCR for ESM1 from HBEC-5i cells
***
**
4
3
2
1
0
IR(8Gy) - + - + - +
Post IR 0 hr 12 hr 24 hr
Time after irradiation
C
IR (8 Gy)
IR+ rhEndocan
IR+ HBEC-5i CM
g1079
Sytox
52%
27.2%
27.9%
Necrotic
Late apoptotic
Viable
Early apoptotic
Casp3/7
D
IR (20 Gy)
IR+ rhEndocan
IR+ HBEC-5i CM
g1051
g1079
Sytox
22.2%
16.2%
14.2%
24.2%
13.4%
12.6%
Caspase 3/7